UCRL-17263

University of California

Ernest O. Lawrence Radiation Laboratory

MEASUREMENT OF THE POLARIZATION PARAMETER IN THE ELASTIC SCATTERING OF NEGATIVE PIONS BY PROTONS FROM 600 TO 3300 MeV/c

TWO-WEEK LOAN COPY

This is a Library Circulating Copy
which may be borrowed for two weeks.
For a personal retention copy, call
Tech. Info. Division, Ext. 5545

DISCLAIMER

This document was prepared as an account of work sponsored by the United States Government. While this document is believed to contain correct information, neither the United States Government nor any agency thereof, nor the Regents of the University of California, nor any of their employees, makes any warranty, express or implied, or assumes any legal responsibility for the accuracy, completeness, or usefulness of any information, apparatus, product, or process disclosed, or represents that its use would not infringe privately owned rights. Reference herein to any specific commercial product, process, or service by its trade name, trademark, manufacturer, or otherwise, does not necessarily constitute or imply its endorsement, recommendation, or favoring by the United States Government or any agency thereof, or the Regents of the University of California. The views and opinions of authors expressed herein do not necessarily state or reflect those of the United States Government or any agency thereof or the Regents of the University of California.

UCRL-17263

UNIVERSITY OF CALIFORNIA

Lawrence Radiation Laboratory
Berkeley, California

AEC Contract No. W-7405-eng-48

MEASUREMENT OF THE POLARIZATION PARAMETER IN THE ELASTIC SCATTERING OF NEGATIVE PIONS BY PROTONS FROM 600 TO 3300 MeV/c

Michel Hansroul

(Ph. D. Thesis)

January 1967

MEASUREMENT OF THE POLARIZATION PARAMETER IN THE ELASTIC SCATTERING OF NEGATIVE PIONS BY PROTONS FROM 600 TO 3300 MeV/c

Contents

Abstract v

I. Introduction 1

II. Experimental Method and Equipment. 3

A. Procedure. 3

B. Pion Beam. 4

C. Polarized Target 8

D. Counter Arrangement. 9

E. Electronics. 12

III. Analysis 16

A. Brief Outline. 16

B. Data Reduction 17

1. Kinematics 17

2. Coplanarity Requirement. 18

3. P and Y Degrees of Freedom. 18

4. Background Subtraction 21

C. Calculation of the Polarization Parameter. 23

D. Errors 27

IV. Results. 29

V. Discussion of the Results. 52

A. Formalism. 52

B. Phase-shift Analyses 55

Acknowledgments 59

Appendix 60

References 64

MEASUREMENT OF THE POLARIZATION PARAMETER IN THE ELASTIC SCATTERING OF NEGATIVE PIONS BY PROTONS FROM 600 TO 3300 MeV/c*

Michel J. Hansroul

Lawrence Radiation Laboratory
University of California
Berkeley, California

January 1967

ABSTRACT

The polarization parameter in $\pi^- p$ elastic scattering has been measured at eleven incident-pion momenta ranging from 600 to 3300 MeV/c. The negative pion beam was focused on a polarized proton target and the scattered pion and recoil proton were detected in coincidence by counter hodoscopes. The polarization parameter was obtained from a measurement of the difference in counting rates for the target protons' spins parallel and antiparallel to the normal to the scattering plane. An on-line PDP-5 computer was used in the data encoding and transferred the information onto magnetic tape for later computer analysis. The results serve to fill in some gaps in previous experiments. An attempt to fit the new data and previously available data by means of a phase-shift analysis for energies below 1050 MeV has been successful in finding good fits to the data but has been unsuccessful in that no unique solution has been demonstrated.

---

* Work done under auspices of U. S. Atomic Energy Commission.

I. INTRODUCTION

In recent years, a considerable amount of experimental data has been obtained for pion-nucleon scattering. As a result, substantial progress has been achieved in establishing the phenomenology of the pion-nucleon system.

The observables in elastic pion-nucleon scattering are the total cross section, the differential cross section, the recoil-nucleon polarization and the spin-rotation parameters R and A[1] for each of the three commonly observed processes:

$$\pi^+ p \rightarrow \pi^+ p$$

$$\pi^- p \rightarrow \pi^- p$$

$$\pi^- p \rightarrow \pi^0 n \ .$$

Due to conservation of total isotopic spin in pion-nucleon interactions, the scattering amplitudes for these three reactions are not independent and can be expressed as linear combinations of two amplitudes corresponding to definite total isotopic spin $T = 3/2$ and $T = 1/2$.

The outstanding feature of the pion-nucleon system is the occurrence of resonant states which appear as enhancements (or bumps) in total cross section measurements.[2-10] For kinetic energies below 300 MeV where inelastic processes play a relatively minor role, several phase-shift analyses have been performed successfully and a unique solution has been found which has been well explained by the partial-wave-dispersion relations.[11] The main result of these analyses is that all the low-energy phenomena in the pion-nucleon system are dominated by the well-known resonance N^* (1236) in the $T = 3/2$ and $J = 3/2$ state, occurring at a kinetic energy of 195 MeV (total center-of-mass energy for the π-N

system = 1236 MeV). At energies above the threshold for inelastic processes, the number of independent parameters becomes considerably bigger, making it necessary to have a very large number of experimental data in order to overcome the increased difficulty of the problem. Fortunately, extensive experimental results coming from differential-cross-section measurements for $\pi^{\pm}p$,[12-14] angular distributions for charge-exchange scattering,[15,16] and recoil-nucleon polarization,[17-19] have recently become available.

With the help of these new data, several groups of researchers have extended the phase-shift analysis of the pion-nucleon system to 1 GeV.[20-25] The results of these analyses have revealed a very complex structure of resonances, many of which were not previously known to exist. The bumps observed in the total cross-section measurements at 600 and 900 MeV, appeared to be due to several resonances, in contrast with the bump at 195 MeV which is explained by the presence of a single resonance, the N^* (1236).

This experiment and a similar experiment for π^+p scattering,[26] were designed to complement existing data and provide additional data which could be used in refining the existing phase-shift solution and extending it to higher energies. In order that our measurements could be used most efficiently, they were taken at incident momenta where differential cross-section measurements already exist. It is hoped that the data taken at the higher momenta ($\geq$ 2 GeV/c) will help to establish the quantum numbers of the resonances for which there is evidence in the total cross-section measurements in the momentum range between 2 GeV/c and 4 GeV/c.

II. EXPERIMENTAL METHOD AND EQUIPMENT

A. Procedure

In the interaction of pions with protons, the differential cross section depends on the state of polarization of the target protons' spins and a different scattered intensity can be obtained for different initial state polarizations. This difference in counting rate allows defining an asymmetry which is uniquely related to the polarization parameter, $P(\theta)$. In the experiment reported here, a beam of negative pions of selected momentum was focused on a polarized proton target and the final-state particles were detected with a pair of counter hodoscopes, one above and one below the unscattered beam.

The differential cross section for scattering pions from a proton target of polarization $\vec{P}_T$, is given by

$$I(\theta) = I_0(\theta)[1 + P(\theta)\hat{n} \cdot \vec{P}_T] \qquad \text{(II-1)}$$

where θ is the center of mass scattering angle,

$I_0(\theta)$ is the differential cross section from unpolarized protons,

$\hat{n} = \hat{k}_i \times \hat{k}_f$ is the normal to the scattering plane ($\vec{k}_i$, $\vec{k}_f$ are the pion's initial and final momenta in the center of mass system),

$P(\theta)$ is the polarization parameter.

The asymmetry is then defined by

$$\epsilon(\theta) = \frac{I^+(\theta)-I^-(\theta)}{I^+(\theta)+I^-(\theta)} = P(\theta)P_T \qquad \text{(II-2)}$$

where $I^+(\theta)$ and $I^-(\theta)$ are the scattered intensities for $\vec{P}_T$ parallel and antiparallel to $\hat{n}$, respectively.

Knowing the target polarization P_T, a measurement of the angular distribution of the asymmetry, $\epsilon(\theta)$, as the target protons' spin direction was reversed, yielded the polarization parameter, $P(\theta)$.

B. Pion Beam

A plan view of the beam transport components is given in Fig. 1. The pions were produced in a copper target traversed by the Bevatron external proton beam (EPB). The EPB pulses were delivered every 6 sec, each pulse being spread as uniformly as possible over a time interval of 0.8 sec. For an EPB pulse of 5×10^{11} protons, the associated pion beam pulses ranged from 4×10^5 to 1.3×10^6, depending upon the momentum selected; the maximum intensity was obtained at momenta near 1 GeV/c and decreased slowly with increasing momentum.

The optical properties of the pion beam are schematically shown in Fig. 2. A first focus F_1 in both horizontal and vertical planes was produced half-way between the quadrupole doublets Q_2 and Q_3. Because of the momentum dispersion induced by the first two bending magnets M_1 and M_2, there was a continuous distribution of images of the production target in the horizontal plane at the first focus, which was nearly recombined at the second focus, F_2, by the action of the bending magnet M_3. As shown in Fig. 1, a counter hodoscope, having 3 overlapping counters P_1, P_2, and P_3 placed at the first

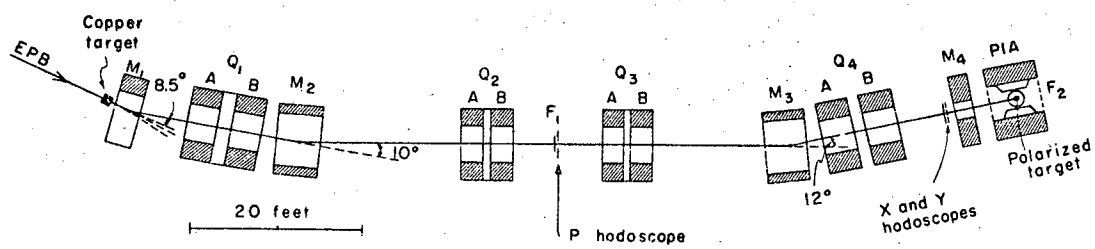

Beam layout

MUB-14038

Fig. 1.

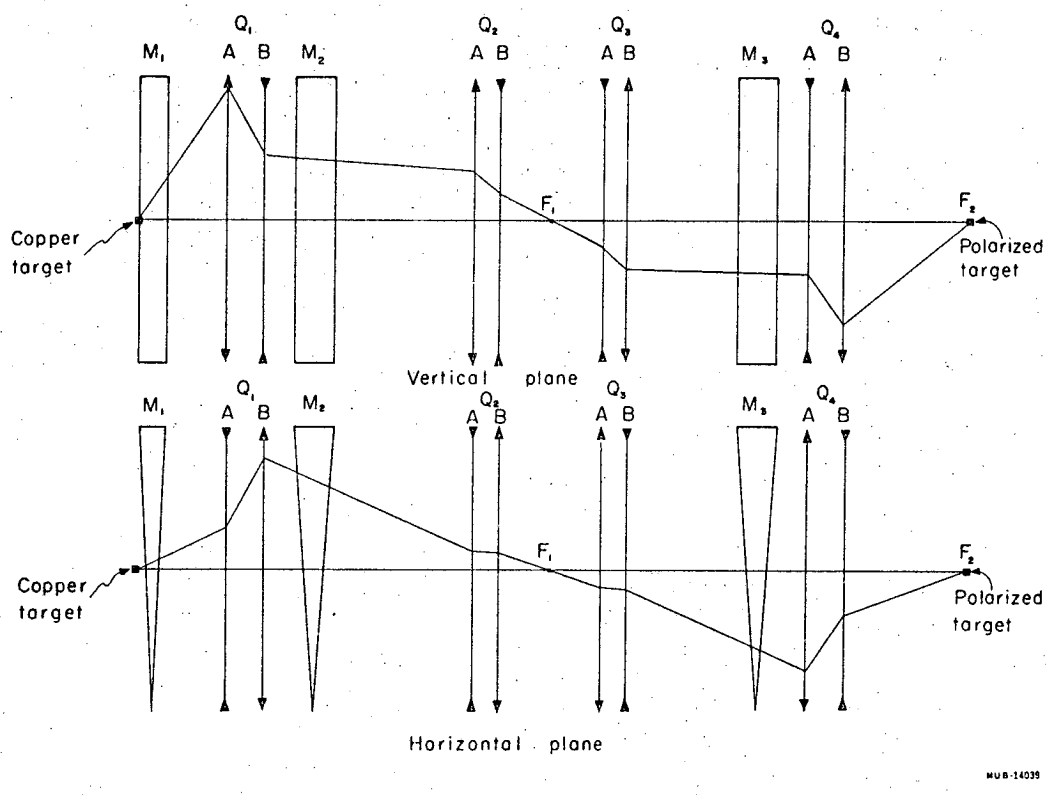

Fig. 2. Beam optics

focus, divided the momentum band ($\Delta P/P \simeq \pm 3\%$) in 5 smaller bands of about $\pm$ 1%, which were treated separately in the analysis of the data. The last quadrupole doublet, Q_4, focused the pion beam on the polarized target crystals, at F_2. The angular convergence of the pions on the target was measured in both the horizontal and vertical planes by a pair of counter hodoscopes, each having 3 counters, labelled X_1, X_2, X_3 in the horizontal plane and Y_1, Y_2, Y_3 in the vertical plane.

In order to cover a large angular region in the center-of-mass system, data were taken for both polarities of the polarized target magnet, Pia. It was thus necessary to place a vertical bending magnet M_4 immediately before Pia to compensate for the deflection of the incident beam by the large magnetic field inside Pia.

The beam was transported in a vacuum up to the exit of Q_4, except for a small distance at the first focus, F_1. The current settings of the magnets Q_3, M_3 and Q_4 were determined by wire-orbit measurements, whereas those of the other magnets were varied to obtain the best beam profiles. The latter were nearly Gaussian in shape, with their full-width at half maximum of about 1.5 in. and 1 in. for the horizontal and vertical profiles, respectively.

The precise values of the mean pion lab momenta at which data were taken were .596, .671, .745, .820, .895, 1.155, 1.352, 1.988, 2.535, 2.912, and 3.260 GeV/c, with an error estimated at 1/2%. These values were determined by 2 sets of wire-orbit measurements, one taken at the beginning of the experiment, the other at the end. These 2 sets were in excellent agreement and were also checked by time-of-flight measure-

ments. In addition, the energy of the proton beam, obtained when the polarity of all the magnets was reversed, was measured by a range telescope. The incident momenta measured by these different methods were all consistent with each other to within 1%.

C. Polarized Target

A detailed description of the polarized proton target used in this experiment can be found in the review article by G. Shapiro,[27] where additional references are listed.

The target consisted of 6 crystals of $La_2Mg_3(NO_3)_{12} \cdot 24\ H_2O$ where a small percentage of the lanthanum had been replaced by neodymium as paramagnetic centers. The high polarization of the neodymium ions in the 18.5 Kilogauss magnetic field at a temperature of 1.0° K was transferred to the free protons of the water of hydration by the method of dynamic nuclear orientation, in which the crystals are irradiated with microwave power of appropriate frequency (70 GHz). The polarization of the target was reversed in sign about once every two hours during the data taking periods, by changing the microwave frequency by a very small amount.

The detection of the polarization was done by the technique of nuclear magnetic resonance (NMR). The proton NMR signal at 78 Mc/sec was repeatedly recorded (about once every 10 minutes) and later compared with the NMR signals obtained when no microwave radiation was applied to the crystals (thermal equilibrium signal). The temperature of the crystals was measured while taking the thermal equilibrium signals. The temperature and frequency measurements gave the absolute calibration of the

polarization of these signals, which is a known function of temperature for a given magnetic field. The average free proton polarization obtained during the experiment was 50%. The errors in the evaluation of the target polarization will be discussed in a later section.

D. Counter Arrangement

The counter arrangement used is shown schematically in Fig. 3. The incoming beam was defined by the P, X and Y hodoscopes, mentioned in Section II-B. Anticoincidence counters were placed to the left and right of the target, as well as immediately above and below it, leaving in front of the crystals an open area slightly bigger than 1 inch square. These counters were used to eliminate a large fraction of possible events coming from interactions in the walls of the cryostat and in the liquid helium surrounding the crystals. They also provided a constant monitoring of the horizontal and vertical positions of the beam while data were taken. Three additional counters were operated in anticoincidence: two of them, not shown in the figure, covered the pole tips of the polarized target magnet and the third, called backup anticounter, counted the pions which had not been scattered in the target. The counter D_d (Down defining) was designed so as to be missed by pions in the beam, but to be traversed by any particle scattered from the target into the lower array of counters.

The scattered pion and recoil proton were detected by two counter hodoscopes, as indicated in Fig. 3. The upper hodoscope consisted of 3 arrays of counters and covered the lab angles between 0 and 45 degrees; it had 30 θ counters, labelled "θ_{up}", which were overlapped so as to

produce a total of 56 bins. These bins defined the scattering angles of the reaction. Similarly, the lower hodoscope consisted of 30 θ counters, labelled "θ_{down}", giving a total of 59 bins which covered the lab angles from 34 to 128 degrees below the beam. In addition to the θ counters, each hodoscope had overlapping stripe counters placed behind the θ counters. These counters served to define bins in the φ direction of a spherical coordinate system with Z axis along the beam direction and were used to apply coplanarity requirements on the accepted events (see Section III). The upper hodoscope had 10 stripe counters, labelled "φ_{up}", giving 19 φ bins, whereas 6 counters, labelled "φ_{down}", defined 11 φ bins in the lower hodoscope.

The lengths and positions of the counters were designed to cover the full solid angle allowed by the separation of the pole tips of Pia. Several factors were considered in the determination of the bin widths in the counter hodoscopes: multiple Coulomb scattering within the crystals, the finite size of the target (1" × 1" × 1.5"), the need for suppression of the background due to scatterings from heavy elements in the target, and the requirement of good angular resolution for the entire range of incident momenta. The two counter hodoscopes were left in fixed positions for all the beam momenta of this experiment. The upper counter hodoscope was about 180 inches from the polarized target.

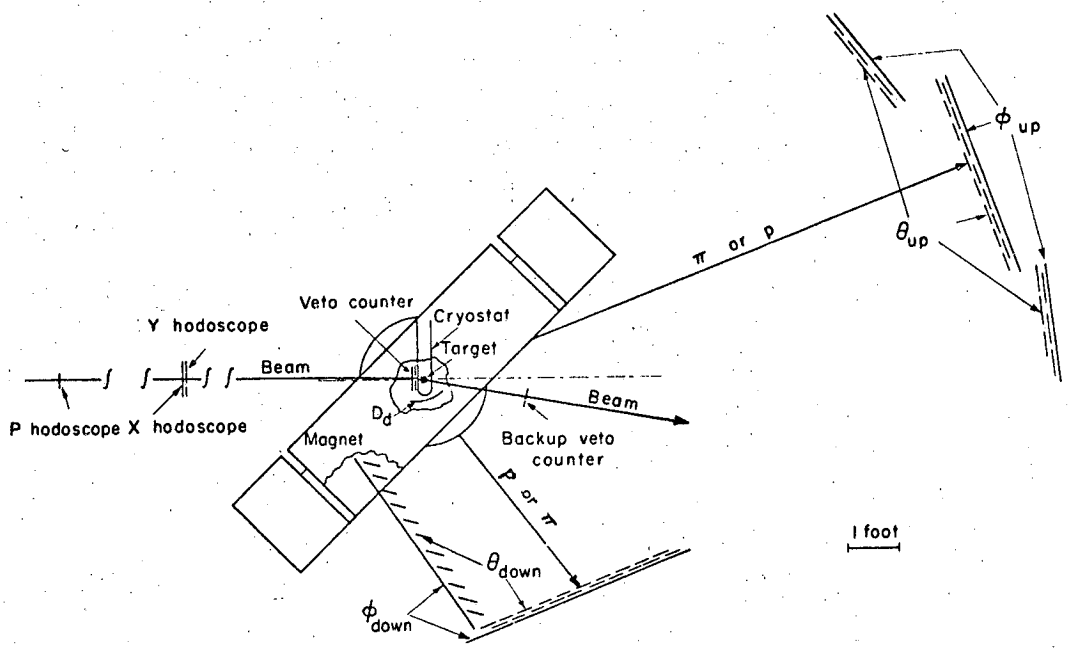

Experimental arrangement

MUB-14036

Fig. 3.

E. Electronics

A block diagram of the electronics is shown in Fig. 4. The signals from the counters were fed into 10 Fast Logic Boxes (FLB), where, after being discriminated, they were each split into two: one part was stored in a long delay line (80 nsec), the other was mixed and sent to the fast trigger circuit. These signals were mixed so as to produce 4 groups of outputs: the sum of all θ_{up} signals, the sum of all θ_{down}, the sum of all φ_{up} and the sum of all φ_{down}. These 4 signals were then used in the fast trigger circuitry to decide when there was an event of interest. The fast trigger logic required a multifold coincidence between the counters of the P, X, Y hodoscopes, D_d, and each of the 4 outputs from the final-state hodoscopes. The various veto counters, mentioned in the previous section, were also part of the fast trigger logic. Therefore, a coincidence in the fast trigger circuit indicated that a pion had interacted in the target to produce at least one charged particle moving through D_d and the lower hodoscope, and at least one charged particle traversing the upper hodoscope. The resolving time of the fast trigger was 20 nsec.

When a trigger occurred, an interrogate pulse was sent back to the fast logic boxes to open a gate at the end of the delay lines, thus allowing the stored signals to set short memory flip-flops. At the same time, the on-line PDP-5 computer was notified via the Data Break Control unit, that an event had occurred. This event was then given an address and stored in the core memory of the PDP-5 via the Data Merger. One event consisted of 8 core words of 12 bits each, specifying which counters had fired. As many as 128 such events could be stored in

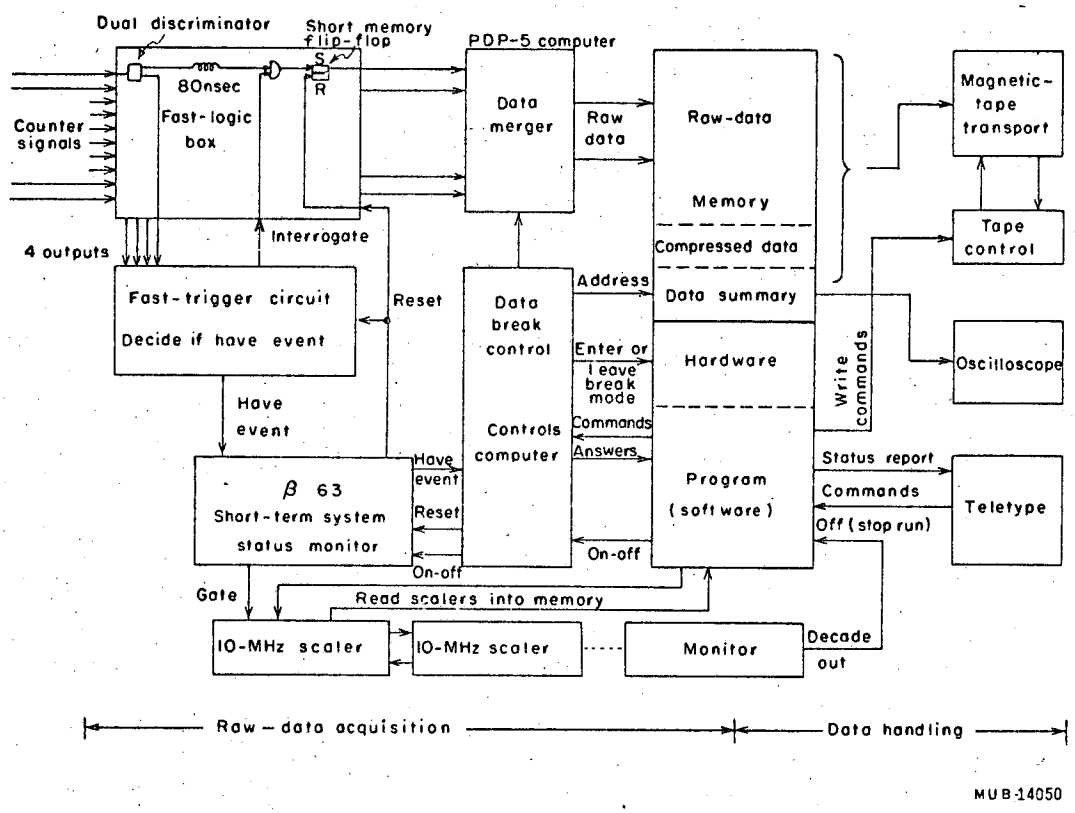

Fig. 4. Electronics block diagram.

the memory before it was full, at which time the information accumulated was written on magnetic tape.

When the computer was not busy storing the raw data, it performed various operations such as decoding the raw data and putting it in more compact form, scaling the counts registered by each of the individual bins and recording the number of invalid triggers. The latter were of two kinds, the "invalid zero" which occurred when there was no signal reaching the computer from any of the required counters (e.g., when no θ_{up} counter recorded a pulse even though the θ_{up} sum signal was present) and the "invalid > 1" which had more than one coincidence for a given trigger. All this information was also written on magnetic tape.

The PDP-5 also prepared summaries of the data that could be displayed on an oscilloscope upon request by the experimenter. With the help of these displays, any anomaly that might have occurred during the data taking periods could immediately be spotted and its cause investigated, before proceeding further with the accumulation of data.

At the end of a running period (typically 15 minutes), the contents of various monitor scalers such as the number of beam particles, the number of counts in the left, right, top and bottom veto counters, the number of accidentals etc . . . were written on the magnetic tape, along with a number identifying the "run" and comments made by the experimenter via the teletype.

Typical trigger rates are listed in Table I. The number of "invalid zero" events was always small (less than 4%), but the "invalid > 1" events could go up to 25% at high incident energies. These rejected triggers did not depend on the beam rate and could be attributed to

genuine multiparticle final states.

Table I. Typical Trigger Rates

P_{lab} (GeV/c)	pions/pulse	triggers/pulse	Invalid zero	Invalid > 1
.745	6.5×10^5	14	2%	18%
1.352	1.34×10^6	40	1.5%	15%
2.535	8.5×10^5	76	3%	22%
3.260	6.4×10^5	64	3%	25%

III. ANALYSIS

A. Brief Outline

The analysis of the PDP-5 output tapes was done on a CDC-6600 computer. Each event appeared on the PDP-5 tape as a set of 7 bin numbers:

θ_{up}	,	varying from 1 to 56
θ_{down}	,	varying from 1 to 59
φ_{up}	,	varying from 1 to 19
φ_{down}	,	varying from 1 to 11
P	,	varying from 1 to 5
X	,	varying from 1 to 3
Y	,	varying from 1 to 3 .

The dimension of the coincidence matrix was thus

$$56 \times 59 \times 19 \times 11 \times 5 \times 3 \times 3 \times \simeq 3 \times 10^7.$$

Clearly, such a large number of degrees of freedom could not be handled directly, even with the largest computers presently available, and it was thus necessary to apply a reduction procedure. Constraints imposed by the kinematics of the reaction and coplanarity requirements were used to reduce this huge matrix into two 56×30 $\theta_{up} - \theta_{down}$ coincidence matrices, one for the pion going up and the other for the pion going down. From each of these matrices, it was then possible to obtain the distribution of coincidences in each θ_{up}

bin as a function of θ_{down} bins and extract from it the elastic events, which were used in the calculation of the polarization parameter.

B. Data Reduction

1. Kinematics

A precise knowledge of the polarized target magnet field contours allowed the calculation of the final-state particles' trajectories for elastic $\pi^- p$ scattering. Combined with accurate position measurements for all the counters, these trajectories determined, for each θ_{up} bin, its corresponding center-of-mass scattering angle and its conjugate θ_{down} bin. As the final-state particles had opposite charge, the magnetic field of Pia provided a convenient kinematic separation between elastic events where the scattered pion reached the upper or lower array of counters. Therefore, for each incident momentum, two kinematic tables were constructed: one contained, for each θ_{up} bin, its corresponding center-of-mass scattering angle and predicted conjugate θ_{down} bin for pions going up, and the other the same quantities for pions going down.

The first step in the analysis was then to classify all the events according to whether the pion was going up or down. This first reduction was accomplished by restricting the range of θ_{down} bins considered to 15 on either side of the predicted elastic scattering bin for a given θ_{up} bin. The fact that the predicted bins for pions going up and down were always at least 30 bins apart, made this constraint unambiguous.

2. Coplanarity requirement

As part of the procedure to reduce the size of the coincidence matrix, we required that the momenta of the incident pion, the scattered pion and the recoil proton lie in the same plane. The incident pion momentum direction in the horizontal plane was determined by the X hodoscope counters, as mentioned in Section II-B, whereas the θ_{up} and φ_{up} bins defined the momentum direction of the final-state particle reaching the upper counter array. Then, for a given θ_{down} bin, the coplanarity constraint determined the corresponding φ bin in the lower counter array. In practice, due to the finite size of the bins and target, events were considered coplanar, if the final-state particle hit the lower array within a small region (typically 2 to 4 bins) centered at the φ bin determined in the manner just described. This method provided a means of classifying the events in 2 categories, coplanar and non-coplanar, thus eliminating the degrees of freedom corresponding to φ_{up}, φ_{down} and X.

Aside from reducing the number of degrees of freedom, the coplanarity requirement was a major factor in removing a large fraction of the background coming from scattering on heavy elements in the target. Actually, the size of the coplanar stripe was chosen so as to give a good ratio of events from free protons to background events without rejecting a large fraction of free-proton events.

3. P and Y degrees of freedom

As was mentioned in Section II-B, the beam was analyzed into 5 momentum bands of ± 1% by the P counter hodoscope. A correction was introduced for the events occurring in the off-central-momentum bands, which took this difference in incident momentum into account. This correction was

evaluated by calculating, for a given θ_{up} bin, the change in the conjugate θ_{down} bin number predicted by kinematics due to this difference in incident momentum, and then adjusting the θ_{down} bin number of the event considered by this computed number. The modification so introduced was very small, the biggest change in the θ_{down} bin number never exceeding 2 units.

Similarly, the angular convergence of the beam in the vertical plane, measured by the Y counter hodoscope, was taken into account by a rotation of the events in the vertical plane; but, in this case, the rotation affected both final-state particles. This correction was also fairly small, amounting to a maximum of 3 units for the change in bin numbers.

The analysis proceeded by examining one event at a time and applying to it the various constraints which successively eliminated the X, φ_{up}, φ_{down}, P and Y degrees of freedom. The events were then scaled in their appropriate element in one of the two 56×30 $\theta_{up} - \theta_{down}$ coincidence matrices (one for pion going up, the other for pion going down), which were subsequently used in the final computation of the polarization parameter. Typical distributions of counts obtained for coplanar events are shown in Fig. 5. They represent the coincidence rates in some of the θ_{up} bins as a function of the θ_{down} bin number. The elastic scattering events on free protons stand out clearly above the background of inelastic or quasi-elastic scattering from bound protons in the heavy elements of the target, despite the fact that the free protons in the target contribute only to 3% of the total weight of

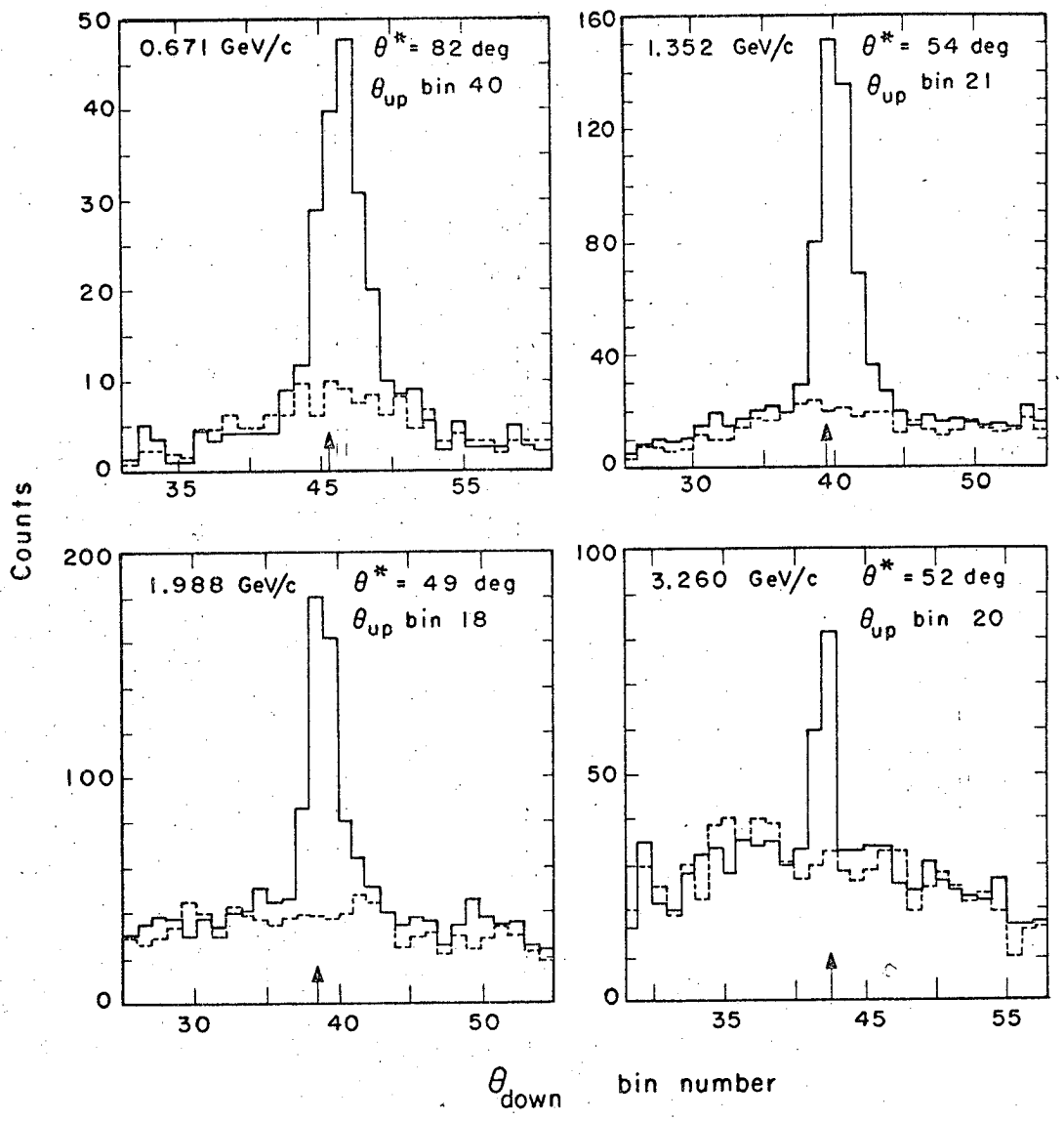

MUB-14035

Fig. 5. Typical distributions of counts. The solid and dashed lines correspond to coplanar and non-coplanar events, respectively. At each energy, the data for both curves were collected simultaneously and thus normalized to the same cumulative amount of incident beam.

the crystals.

4. Background subtraction

The evaluation of the background under the elastic peak was done by using events which did not satisfy the coplanarity requirement. The selection of these events was obtained under exactly the same conditions which prevailed in the choice of coplanar events, except that they were required to be non-coplanar. Events chosen in this manner were due to inelastic scattering and quasi-elastic scattering from bound protons which had a small transverse component of Fermi momentum. As shown by the dashed lines in Fig. 5, the distribution of these events matched that for coplanar events in the regions outside the elastic peak. In order to verify the validity of this method of background subtraction, data were taken at some beam momenta with a dummy target which was similar to the crystals in every respect, except that it contained no free protons. Results obtained with the dummy target were in complete agreement with those from the non-coplanar events.

A very serious background problem, discovered during the experiment, was the electron contamination of the beam. Although relatively small, it was the cause of a very large background which obscured the elastic pion-proton scattering. The electrons in the beam, when passing through the polarized target crystals, emitted radiation by bremsstrahlung; the photons were subsequently converted in the target by production of electron-positron pairs with momenta parallel to the beam momentum. The electron and positron were then each deflected by the polarized target magnet into the final-state hodoscopes. These "events" had good coplanarity and their rate was especially high for beam momenta

below 1 GeV/c. This "electron background" was eliminated by inserting approximately one radiation length of lead (1/4 inch) at the first focus of the beam, immediately in front of the P counter hodoscope. The energy loss of the pions in the lead was compensated by tuning the magnets in the first leg of the beam for a slightly higher energy. The data at high momenta (2 GeV/c and higher) were not taken with lead in the beam path. Likewise, the data for backward angles (in the center-of-mass system) at the lower incident momenta (below 900 MeV/c) did not suffer from this "electron background", although no lead was used for them.

C. Calculation of the Polarization Parameter

In the previous section, it was shown how the raw data were reduced to a 56 × 30 coincidence matrix. Each row of this matrix represents a distribution of counts such as those shown in Fig. 5. After subtraction of the background, the number of events in the elastic peak can be used to determine the asymmetry in pion-proton scattering by comparing the contribution to this peak of events obtained for positive and negative target polarization (positive target polarization corresponds to the protons' spins predominantly aligned in the direction of the magnetic field).

The data from a set of runs taken under similar circumstances (beam momentum, accidental rate, sign of the polarized target magnetic field) were analyzed together. Each run was monitored by the number of events in that run occurring outside the elastic peak regions of the 56 × 30 matrix. The background was obtained from the non-coplanar events, normalized so that their sum over the off-elastic-peak regions would be equal to the sum of coplanar events in the same regions of the coincidence matrix. The monitor and background were verified to be independent of the target polarization.

Denoting by $N_i(\theta^*)$ the number of counts for the ith run recorded in the elastic peak for a given θ_{up} bin corresponding to the c.m. angle θ^*, one can write from (II-1)

$$N_i(\theta^*) = M_i \, I_0(\theta^*) \left[1 + p_i \, P(\theta^*) \right] + B_i \qquad \text{(III-1)}$$

where

M_i = number of monitor counts during i^{th} run

$I_0(\theta^*)$ = unpolarized differential cross section times the solid angle subtended by the θ_{up} bin considered, normalized to unit monitor

p_i = algebraic value of the target polarization during the ith run

$P(\theta^*)$ = polarization parameter

B_i = contribution of the background counts in the elastic peak during the ith run.

The number of background counts is obtained from the number of non-coplanar events in the elastic peak, D_i , normalized to the off-elastic region of the matrix. The normalization factor is then

$$R = \frac{\sum_i \sum_{NE} N_i}{\sum_j \sum_{NE} D_j}$$

where the sums over i and j denote sums over all runs used for coplanar and non-coplanar events, respectively; NE indicates a sum over the off-elastic-peak regions. Then B_i can be written as

$$B_i = M_i\ b = M_i\ R\ \frac{\sum_j \sum_{EP} D_j}{\sum_i M_i} \qquad \text{(III-2)}$$

where b is the number of background counts per unit monitor in the elastic peak, and $\sum_{EP} D_j$ represents the sum of non-coplanar events in the elastic peak during the jth run.

The monitor used for each run was the number of coplanar events outside the elastic peak region,

$$M_i = \sum_{NE} N_i \quad .$$

From (III-1) the number of counts per unit monitor, H_i, due to scattering from free protons, can be written

$$H_i = \frac{N_i - B_i}{M_i} = I_0(\theta^*) \left[1 + p_i \; P(\theta^*)\right].$$

This expression shows that H_i is a linear function of the target polarization, p_i. The method of least squares can now be used to determine I_0 and P by minimizing the quantity

$$J = \sum_i M_i \left[H_i - I_0(1 + p_i \; P)\right]^2 \quad . \qquad \text{(III-3)}$$

The factor M_i is a weighting factor proportional to the effective counting time during the ith run. The condition for a minimum of J is

$$\frac{\partial J}{\partial I_0} = \frac{\partial J}{\partial (I_0 P)} = 0 \; . \qquad \text{(III-4)}$$

From (III-4) the polarization parameter, $P(\theta^*)$, can be expressed in terms of the various counting rates and target polarizations. The details of the derivation are given in the Appendix.

The polarization parameter, $P(\theta^*)$, was calculated in this way for each bin in the upper hodoscope. The runs included in the analysis at any one energy were selected for their similar experimental conditions, the number of runs with positive and negative target polarization being about equal.

The center-of-mass scattering angles were calculated by the kinematics, as described in Section III-B; the close agreement between the predicted θ_{down} bin conjugate to a given θ_{up} bin and the position of the elastic peak obtained experimentally justifies complete confidence in our method of calculation (see Fig. 5).

The target polarization for each run was calculated from the nuclear magnetic resonance signal taken during that run. The magnitude of this signal was compared to the thermal equilibrium signals, which were taken about every 12 hours during the running periods. The NMR signals were digitized and recorded on paper tape during the runs. They were then reconstructed and analyzed on a computer. In general, several NMR signals were taken on chart paper during each 15 minute run, only one or two of them being recorded on paper tape. For the majority of the runs, the polarization calculated from the recorded NMR signal was a good measure of the average target polarization for the duration of that run. The variation with time of the magnitude of the polarization was small; its contribution to the errors was included in the systematic error discussed in the next section.

D. Errors

The various contributions to the statistical error in the polarization parameter have been examined in the Appendix. The total statistical error for each θ_{up} bin is determined by the statistical errors in the number of coplanar and background events in the elastic peak, the number of monitor counts and the normalization ratio used for the background subtraction.

In addition to the statistical error, a systematic error common to all the data is due to the uncertainty in the evaluation of the target polarization. The target polarization is obtained from measurements of the following quantities:

(i) Magnitude of the NMR signal when the target is polarized,

(ii) Magnitude of the thermal equilibrium signal,

(iii) Temperature of the crystals while the thermal equilibrium signals are taken.

The temperature of the crystals during the thermal equilibrium signal was assumed to be the same as that of the surrounding liquid helium bath. The liquid helium temperature was obtained from a measurement of the helium vapor pressure by means of a McLeod vacuum gauge. Due to the high precision of this instrument it was estimated that the error in temperature contributed a negligible amount to the total error.

The error in the measurement of the magnitude of the NMR signal from a polarized target is about 2%. An additional uncertainty of about

3% is introduced by the fact that the polarization obtained from the NMR signal recorded during a run does not represent the true average polarization for the duration of that run (about 15 minutes).

The major contribution to the total error comes from the uncertainty in the evaluation of the magnitude of the thermal equilibrium signals. Because of a smaller signal-to-noise ratio, the measurement error is of the order of 5%, as estimated from repeated measurements of the same signal. An additional uncertainty in the thermal equilibrium signals is due to the lack of agreement between signals taken at different times during the experiment. This effect is believed to be due to variations in time of the detection-system properties. The size of this error is estimated at 5%.

These systematic errors were added in quadrature to give a total systematic error of ±8%, to be applied to all the results given in the next section.

IV. RESULTS

The polarization parameter was calculated for each θ_{up} bin in the manner described in Section III-C. In the final results presented in Figs. 6 through 16 and Tables II through XII, the polarization parameter was obtained by averaging over the results of several adjacent θ_{up} bins (in general 2 to 4 bins), each being weighted by the square of the inverse of its statistical error. The errors shown in the figures and listed in the tables are statistical only and do not include the systematic error discussed in the previous section.

The minimum differential cross section for which the polarization parameter could be measured was approximately 50 μb/str in the center-of-mass system. In order that the recoil proton could easily escape the target and traverse the counter hodoscope, it was required to have a momentum of at least 350 MeV/c, thus imposing a lower limit in momentum-transfer for which polarization measurements were feasible.

It is worth mentioning that a measurement of the polarization parameter in proton-proton scattering at 1390 MeV/c was performed using the same detection apparatus as for the pion-proton scattering. The results were in good agreement with previous measurements,[28,29,30] thus certifying the validity of the method used for the background subtraction and the calculation of the target polarization.

At those momenta for which previous measurements have been made, the agreement is good.[17,18,31]

Table II. Polarization parameter $P(\theta)$ in $\pi^- p$ scattering. The error $\Delta P(\theta)$ is statistical only and does not include the systematic error discussed in Section III-D.

P_{lab}=.596 GeV/c	T_{lab}=.472 GeV	E_{cm}=1.431 GeV	
Cos θ_{cm}	-t	$P(\theta)$	$\Delta P(\theta)$
-.666	.516	.64	.28
-.738	.538	.42	.19
-.801	.558	-.08	.23
-.855	.575	.03	.12
-.901	.589	.10	.09
-.936	.600	.20	.08
-.960	.607	.07	.08
-.978	.613	.12	.11

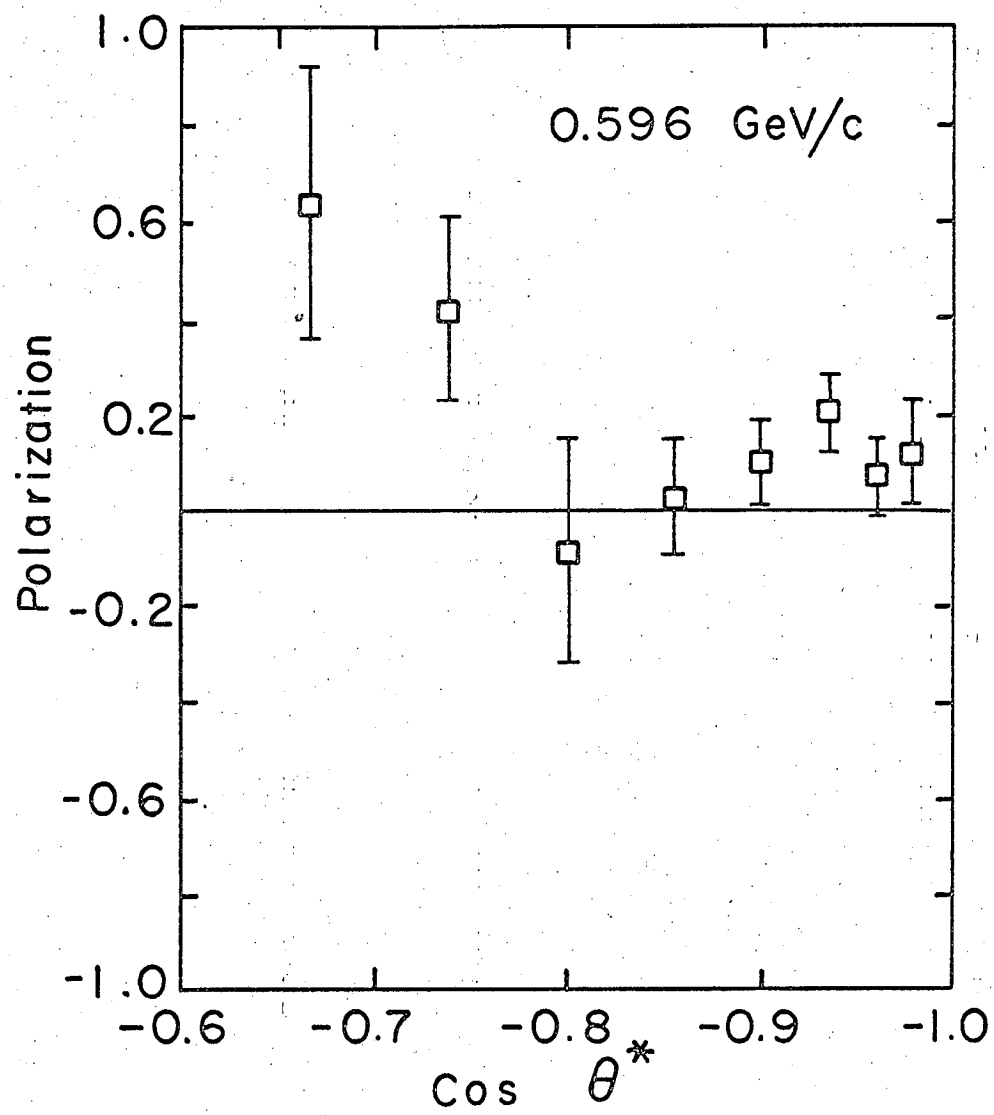

MUB-14037

Fig. 6. Polarization in $\pi^- p$ scattering for an incident-pion momentum of .596 GeV/c. The errors shown are statistical only and do not include the systematic error discussed in Section III-D. The systematic error corresponds to an uncertainty of 8 percent in the target polarization. It results in an 8 percent uncertainty in the scale against which the polarization is measured.

Table III. Polarization parameter $P(\theta)$ in $\pi^- p$ scattering. The error $\Delta P(\theta)$ is statistical only and does not include the systematic error discussed in Section III-D.

P_{lab}=.671 GeV/c	T_{lab}=.545 GeV	E_{cm}=1.478 GeV	
Cos θ_{cm}	-t	$P(\theta)$	$\Delta P(\theta)$
.496	.185	-.62	.19
.444	.204	-.63	.12
.399	.221	-.65	.11
.347	.239	-.89	.09
.289	.261	-.75	.10
.230	.283	-.82	.10
.171	.304	-.88	.09
.113	.326	-.71	.12
.054	.347	-.74	.12
-.031	.379	-.61	.14
-.126	.413	-.20	.17
-.142	.419	.15	.18
-.315	.483	.36	.16
-.481	.544	.39	.25
-.694	.622	-.08	.08
-.762	.647	-.16	.08
-.823	.669	-.08	.07
-.874	.688	-.25	.07
-.916	.703	-.23	.09
-.944	.714	-.39	.12
-.966	.722	-.09	.26

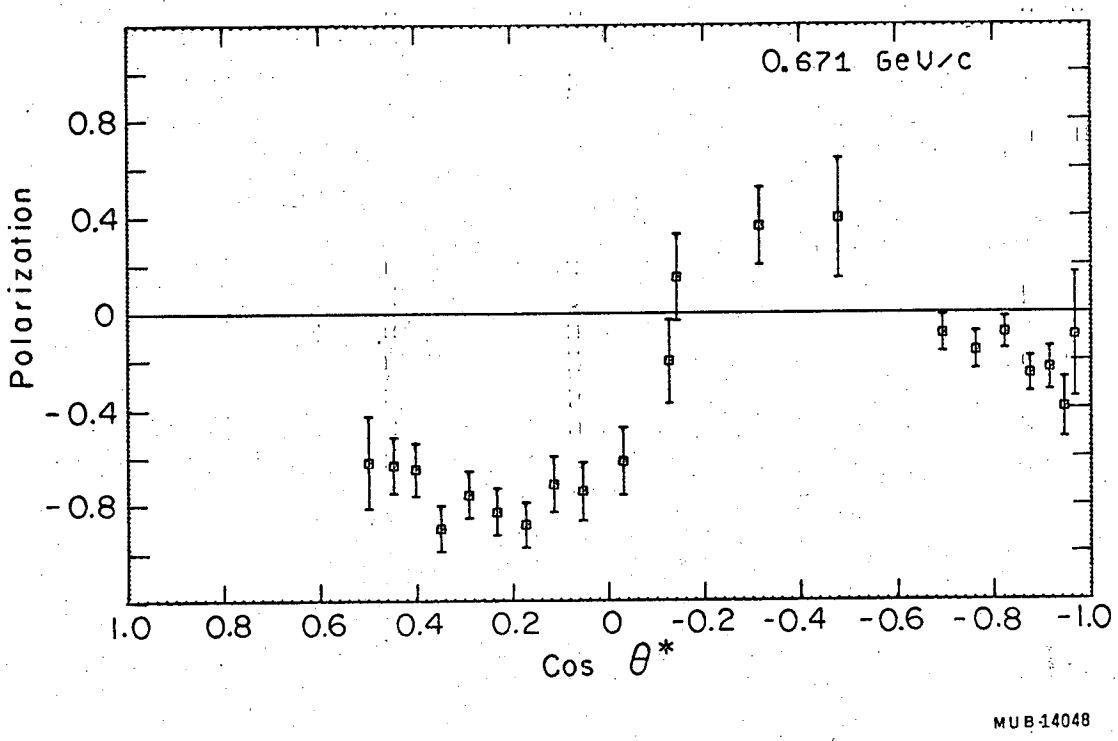

Fig. 7. Polarization in $\pi^- p$ scattering for an incident-pion momentum of 0.671 GeV/c. The errors shown are statistical only and do not include the systematic error discussed in Section III-D. The systematic error corresponds to an uncertainty of 8 percent in the target polarization. It results in an 8 percent uncertainty in the scale against which the polarization is measured.

Table IV. Polarization parameter $P(\theta)$ in $\pi^- p$ scattering. The error $\Delta P(\theta)$ is statistical only and does not include the systematic error discussed in Section III-D.

P_{lab}=.745 GeV/c	T_{lab}=.618 GeV	E_{cm}=1.542 GeV	
Cos θ_{cm}	-t	$P(\theta)$	$\Delta P(\theta)$
.605	.168	-.37	.22
.521	.204	-.53	.11
.477	.222	-.37	.08
.431	.242	-.59	.07
.377	.265	-.54	.07
.317	.290	-.58	.07
.258	.316	-.57	.08
.198	.341	-.64	.09
.139	.366	-.56	.10
.075	.393	-.65	.11
.006	.422	-.40	.14
-.067	.453	-.45	.13
-.091	.464	-.30	.34
-.155	.491	-.07	.25
-.192	.507	.27	.34
-.239	.527	.39	.26
-.313	.558	-.18	.34
-.412	.600	-.04	.18
-.421	.604	-.64	.28
-.479	.629	-.37	.31
-.538	.654	-.64	.27
-.725	.733	-.62	.27
-.774	.755	-.92	.12
-.833	.780	-.92	.12
-.883	.801	-.68	.15
-.921	.817	-.47	.21
-.958	.832	-.59	.25

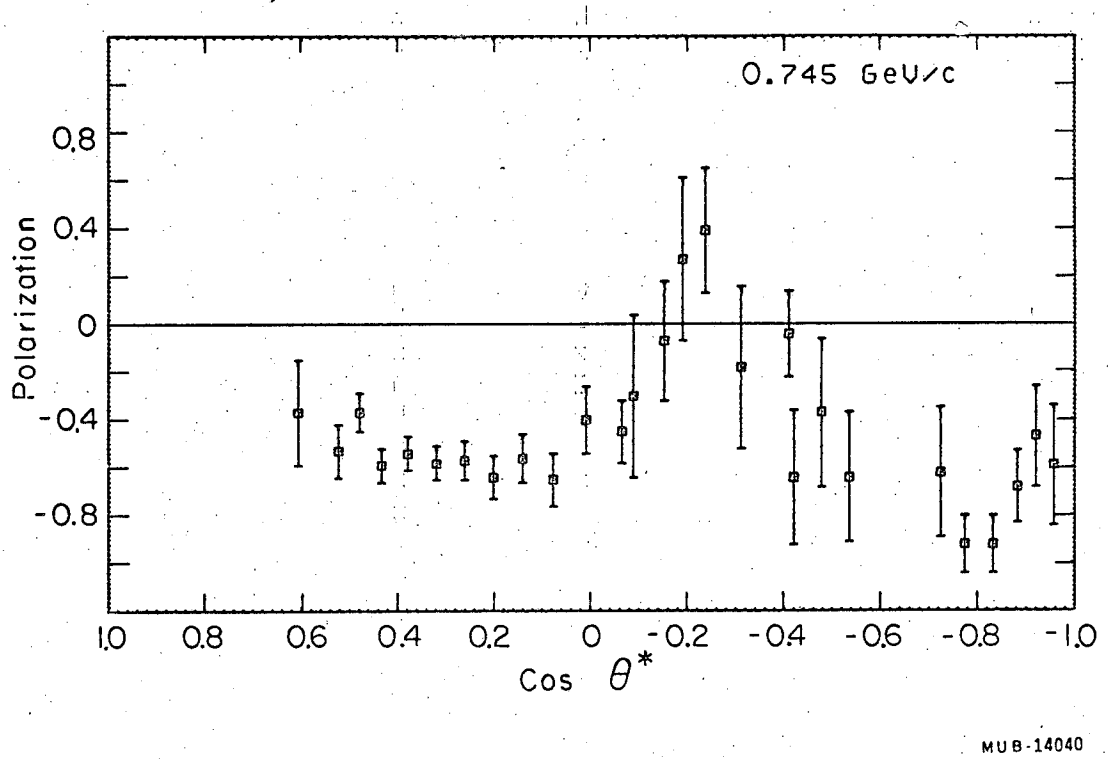

Fig. 8. Polarization in π^-p scattering for an incident-pion momentum of 0.745 GeV/c. The errors shown are statistical only and do not include the systematic error discussed in Section III-D. The systematic error corresponds to an uncertainty of 8 percent in the target polarization. It results in an 8 percent uncertainty in the scale against which the polarization is measured.

Table V. Polarization parameter $P(\theta)$ in $\pi^- p$ scattering. The error $\Delta P(\theta)$ is statistical only and does not include the systematic error discussed in Section III-D.

P_{lab}=.820 GeV/c T_{lab}=.692 GeV E_{cm}=1.569 GeV

Cos θ_{cm}	-t	$P(\theta)$	$\Delta P(\theta)$
.574	.207	-.09	.13
.528	.229	-.27	.11
.488	.248	-.24	.08
.439	.272	-.32	.07
.380	.301	-.24	.08
.320	.330	-.48	.08
.259	.359	-.25	.08
.199	.389	-.30	.10
.139	.418	-.57	.11
.059	.457	-.29	.11
-.040	.505	-.18	.16
-.104	.536	1.00	.42
-.130	.549	.39	.28
-.219	.592	.80	.29
-.342	.652	.41	.25
-.427	.692	.09	.16
-.441	.699	.18	.22
-.505	.731	-.25	.22
-.548	.752	.14	.15
-.620	.787	-.36	.22
-.789	.868	-.57	.09
-.846	.896	-.59	.07
-.893	.919	-.57	.06
-.926	.935	-.68	.07
-.952	.948	-.695	.09
-.965	.954	-.65	.23

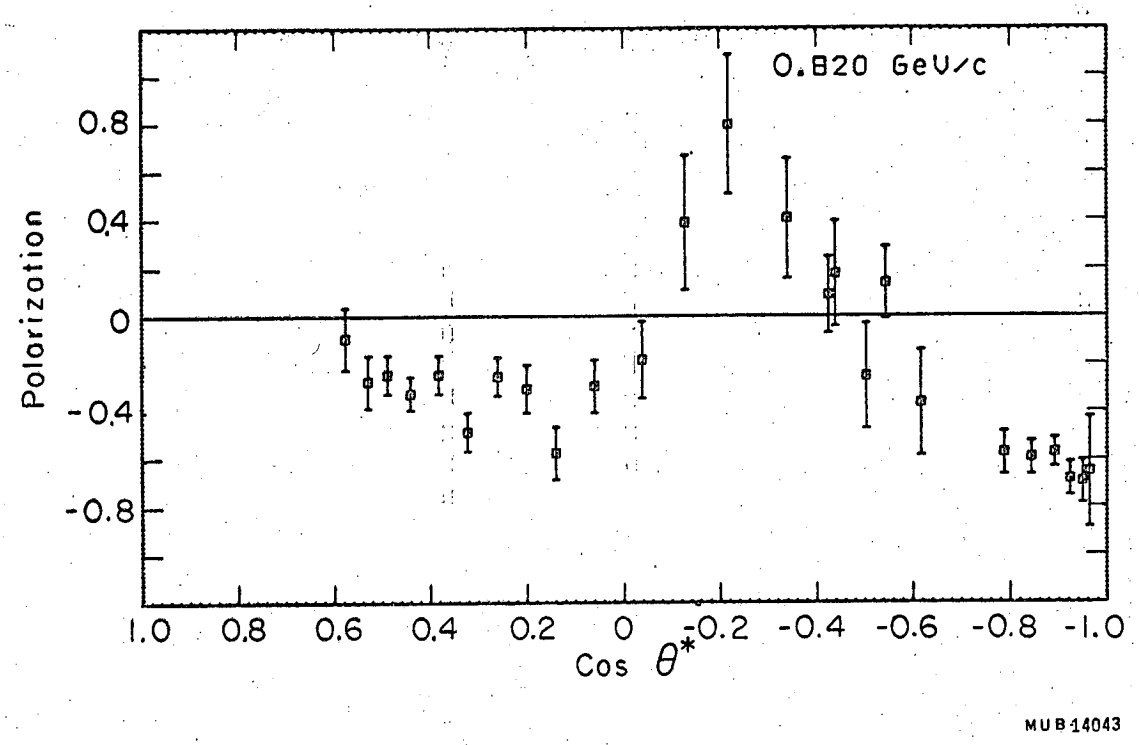

Fig. 9. Polarization in π^-p scattering for an incident-pion momentum of 0.820 GeV/c. The errors shown are statistical only and do not include the systematic error discussed in Section III-D. The systematic error corresponds to an uncertainty of 8 percent in the target polarization. It results in an 8 percent uncertainty in the scale against which the polarization is measured.

Table VI. Polarization parameter $P(\theta)$ in $\pi^- p$ scattering. The error $\Delta P(\theta)$ is statistical only and does not include the systematic error discussed in Section III-D.

P_{lab}=.895 GeV/c T_{lab}=.766 GeV E_{cm}=1.612 GeV

Cos θ_{cm}	-t	$P(\theta)$	$\Delta P(\theta)$
.706	.161	.27	.41
.643	.195	.16	.17
.571	.234	-.10	.12
.526	.259	-.09	.11
.479	.285	-.00	.09
.421	.317	-.20	.09
.360	.350	-.07	.10
.299	.383	.04	.09
.237	.417	-.03	.10
.176	.450	.04	.12
.104	.490	-.15	.12
.004	.545	.14	.14
-.094	.598	-.58	.21
-.215	.664	-.62	.23
-.276	.698	-.32	.14
-.340	.732	.67	.19
-.440	.787	.43	.10
-.509	.825	.42	.14
-.550	.848	.29	.09
-.631	.892	-.11	.09
-.707	.933	.16	.19
-.790	.979	.02	.11
-.820	.995	-.18	.08
-.861	1.017	-.27	.05
-.902	1.040	-.38	.05
-.933	1.057	-.51	.06
-.956	1.070	-.61	.10

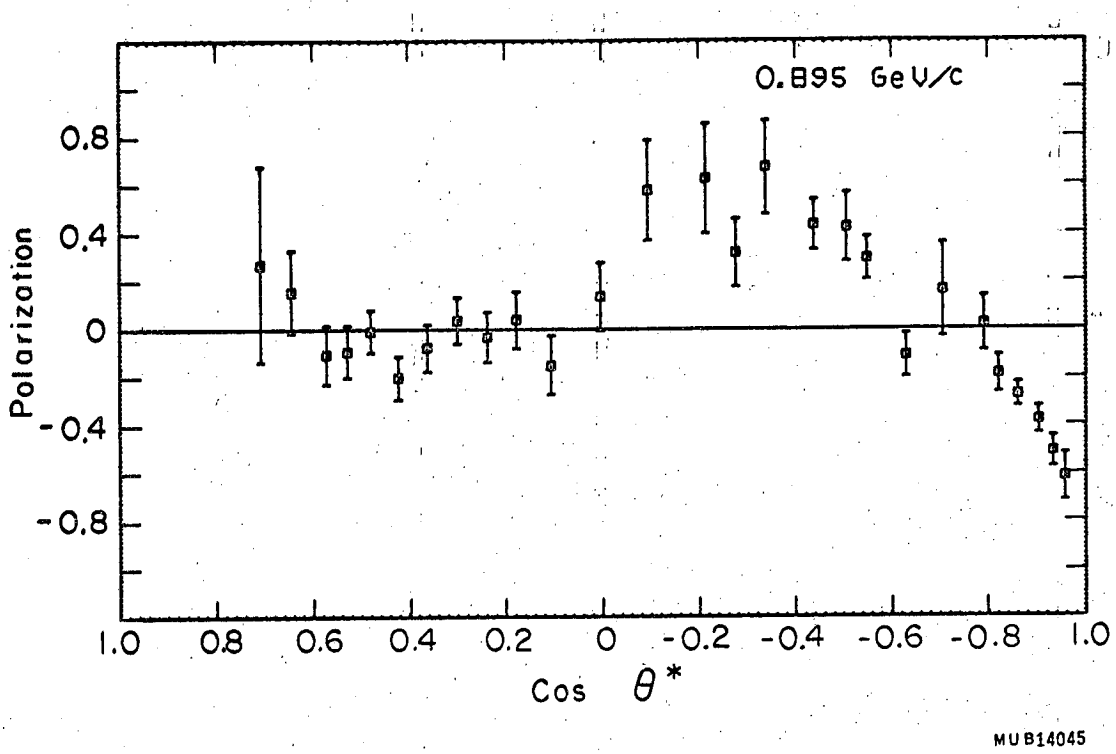

Fig. 10. Polarization in $\pi^- p$ scattering for an incident-pion momentum of 0.895 GeV/c. The errors shown are statistical only and do not include the systematic error discussed in Section III-D. The systematic error corresponds to an uncertainty of 8 percent in the target polarization. It results in an 8 percent uncertainty in the scale against which the polarization is measured.

Table VII. Polarization parameter $P(\theta)$ in $\pi^- p$ scattering. The error $\Delta P(\theta)$ is statistical only and does not include the systematic error discussed in Section III-D.

P_{lab}= 1.155 GeV/c T_{lab}=1.024 GeV E_{cm}=1.756 GeV

Cos θ_{cm}	-t	$P(\theta)$	$\Delta P(\theta)$
.796	.156	-.16	.20
.751	.191	-.05	.12
.710	.222	.17	.12
.647	.270	.27	.09
.614	.296	.18	.08
.579	.322	.24	.09
.542	.350	.17	.09
.498	.384	.35	.10
.444	.426	.23	.12
.380	.475	.13	.17
.315	.524	-.70	.22
.251	.574	-.71	.18
.185	.624	-.97	.16
.090	.696	-.99	.11
-.014	.777	-.93	.10
-.048	.802	-.97	.59
-.095	.838	-.86	.17
-.127	.863	-.63	.22
-.256	.962	-.55	.20
-.380	1.057	-.26	.18
-.462	1.119	-.07	.21
-.534	1.175	-.07	.17
-.605	1.229	.22	.13
-.648	1.262	-.04	.15

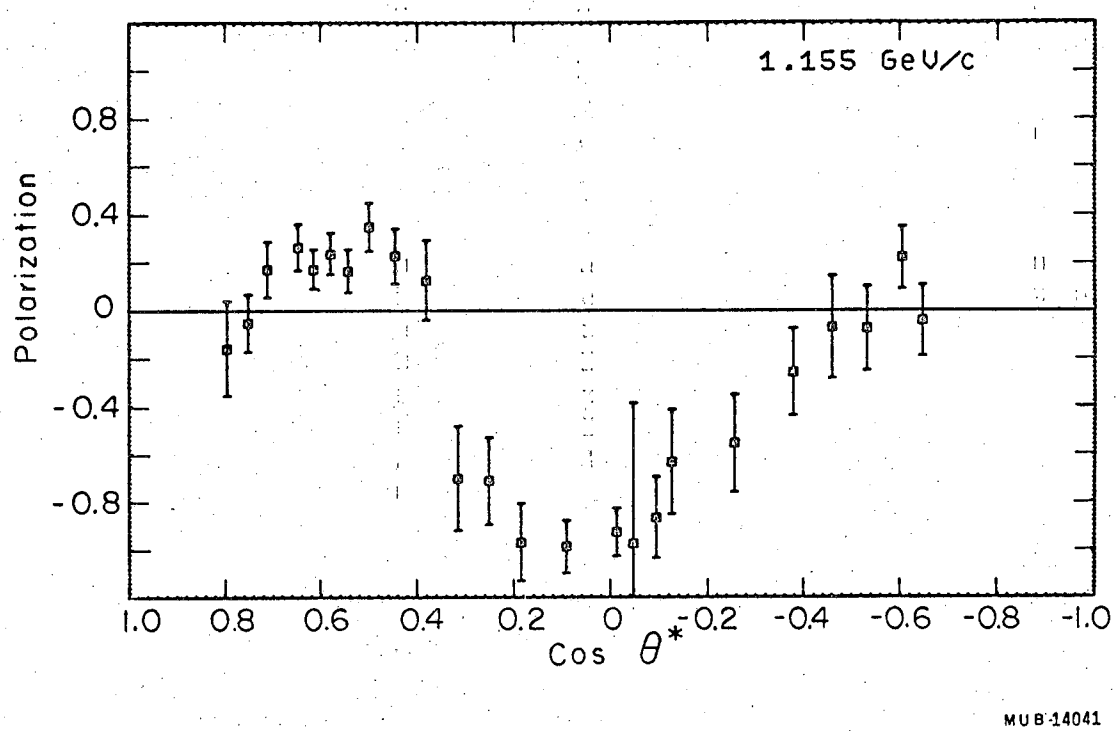

Fig. 11. Polarization in $\pi^- p$ scattering for an incident-pion momentum of 1.155 GeV/c. The errors shown are statistical only and do not include the systematic error discussed in Section III-D. The systematic error corresponds to an uncertainty of 8 percent in the target polarization. It results in an 8 percent uncertainty in the scale against which the polarization is measured.

Table VIII. Polarization parameter $P(\theta)$ in $\pi^- p$ scattering. The error $\Delta P(\theta)$ is statistical only and does not include the systematic error discussed in Section III-D.

P_{lab} = 1.352 GeV/c T_{lab} = 1.220 GeV E_{cm} = 1.857 GeV

Cos θ_{cm}	-t	$P(\theta)$	$\Delta P(\theta)$
.831	.158	-.06	.17
.770	.215	.09	.08
.729	.254	.19	.11
.673	.306	.23	.08
.638	.338	.27	.07
.596	.378	.17	.07
.543	.428	.20	.08
.479	.487	.21	.10
.413	.549	.01	.13
.346	.612	-.27	.18
.279	.674	-.58	.19
.213	.736	-.89	.17
.125	.819	-.89	.11
.016	.921	-1.16	.10
-.048	.981	-1.03	.20
-.082	1.013	-.92	.12
-.170	1.095	-.74	.17
-.302	1.220	-.53	.18
-.409	1.319	-.43	.22
-.485	1.390	-.07	.19
-.559	1.460	-.08	.18
-.631	1.527	.03	.15
-.695	1.587	.13	.15

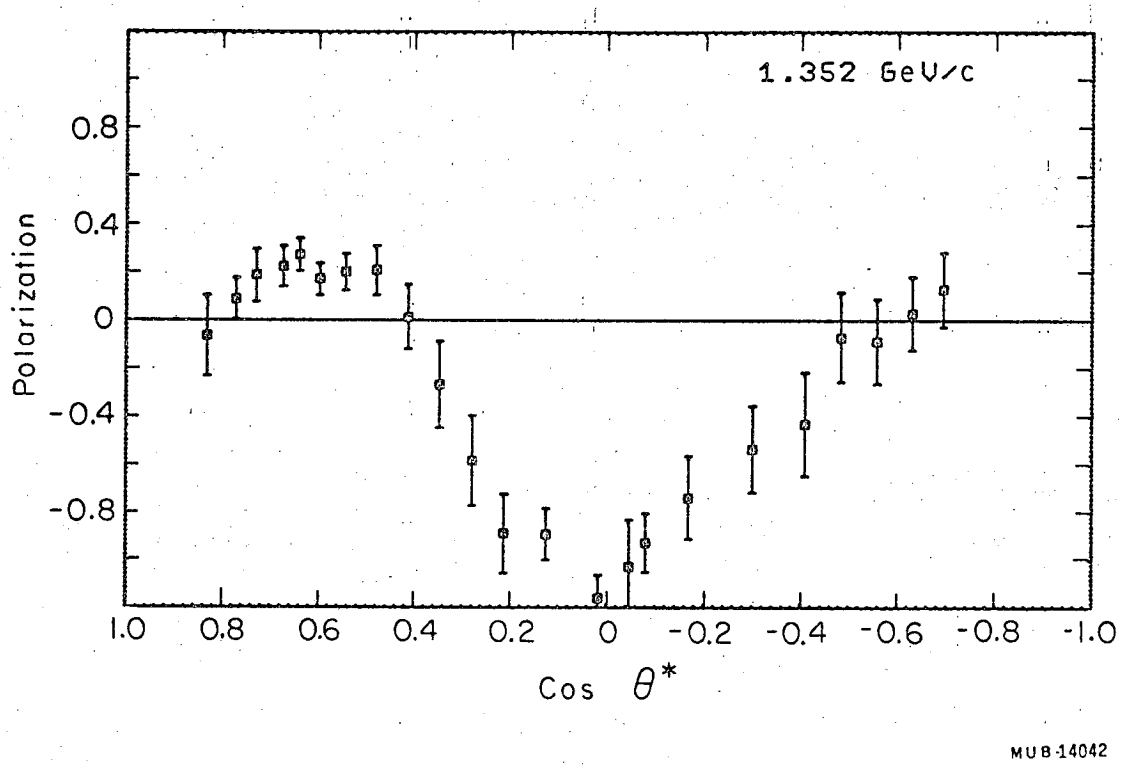

Fig. 12. Polarization in $\pi^- p$ scattering for an incident-pion momentum of 1.352 GeV/c. The errors shown are statistical only and do not include the systematic error discussed in Section III-D. The systematic error corresponds to an uncertainty of 8 percent in the target polarization. It results in an 8 percent uncertainty in the scale against which the polarization is measured.

Table IX. Polarization parameter $P(\theta)$ in $\pi^- p$ scattering. The error $\Delta P(\theta)$ is statistical only and does not include the systematic error discussed in Section III-D.

P_{lab}=1.988 GeV/c	T_{lab}=1.853 GeV	E_{cm}= 2.154 GeV	
Cos θ_{cm}	-t	$P(\theta)$	$\Delta P(\theta)$
.838	.243	-.13	.20
.787	.319	-.03	.07
.709	.438	.15	.07
.671	.495	.13	.08
.631	.554	.49	.12
.589	.617	.46	.13
.539	.693	.35	.13
.485	.774	.21	.12
.429	.857	-.01	.10
.374	.941	-.26	.10
.318	1.024	-.23	.09
.263	1.107	-.27	.08
.208	1.189	-.30	.08
.146	1.283	-.22	.07
.058	1.415	-.30	.07
.024	1.466	-.42	.11
-.028	1.545	-.51	.09
-.076	1.617	-.63	.13
-.111	1.669	-.54	.14
-.180	1.774	-.92	.14
-.284	1.930	-.99	.27
-.357	2.039	-.79	.26
-.419	2.133	-.004	.28
-.471	2.210	-.41	.33

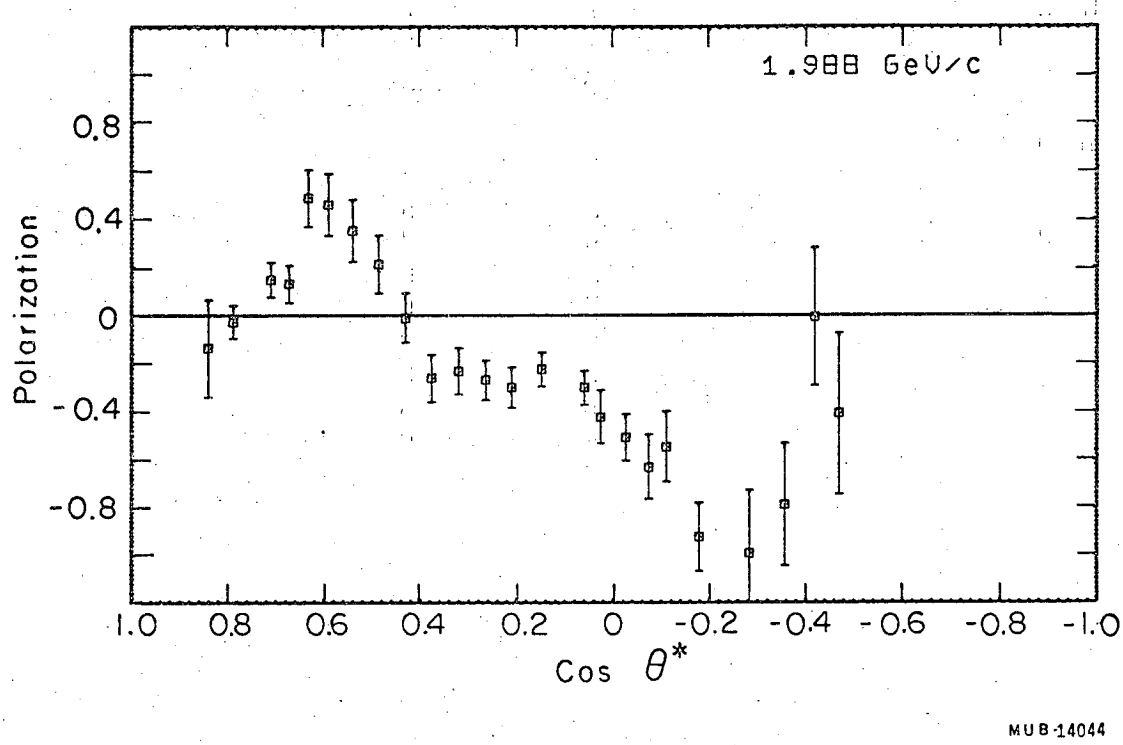

Fig. 13. Polarization in $\pi^- p$ scattering for an incident-pion momentum of 1.988 GeV/c. The errors shown are statistical only and do not include the systematic error discussed in Section III-D. The systematic error corresponds to an uncertainty of 8 percent in the target polarization. It results in an 8 percent uncertainty in the scale against which the polarization is measured.

Table X. Polarization parameter $P(\theta)$ in $\pi^- p$ scattering. The error $\Delta P(\theta)$ is statistical only and does not include the systematic error discussed in Section III-D.

P_{lab}=2.535 GeV/c T_{lab}=2.399 GeV E_{cm}=2.380 GeV

Cos θ_{cm}	-t	$P(\theta)$	$\Delta P(\theta)$
.894	.213	-.08	.14
.854	.291	.007	.09
.810	.379	-.11	.12
.781	.437	.09	.13
.709	.582	.09	.12
.653	.693	-.21	.22
.594	.812	-.55	.21
.522	.957	-.89	.18
.442	1.115	-.90	.13
.362	1.275	-.60	.11
.283	1.435	-.54	.11
.204	1.591	-.21	.11
.121	1.757	-.19	.13
.097	1.806	.22	.16
.003	1.994	.09	.24
-.012	2.025	.16	.20

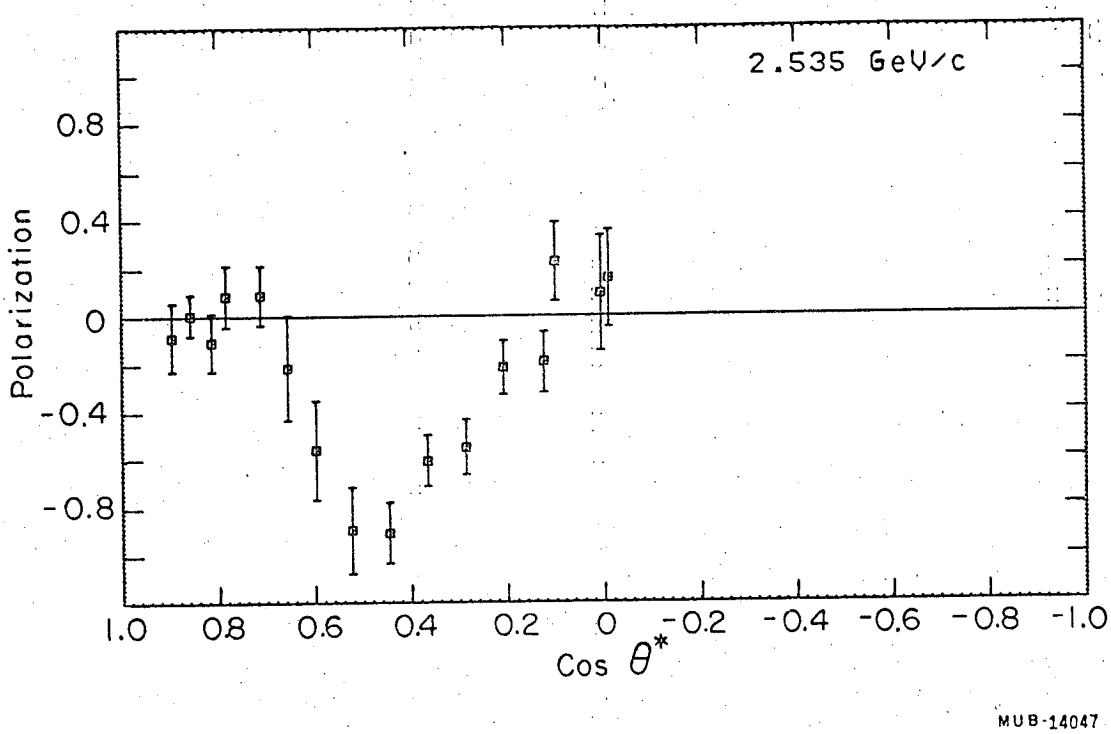

Fig. 14. Polarization in $\pi^- p$ scattering for an incident-pion momentum of 2.535 GeV/c. The errors shown are statistical only and do not include the systematic error discussed in Section III-D. The systematic error corresponds to an uncertainty of 8 percent in the target polarization. It results in an 8 percent uncertainty in the scale against which the polarization is measured.

Table XI. Polarization parameter $P(\theta)$ in $\pi^- p$ scattering. The error $\Delta P(\theta)$ is statistical only and does not include the systematic error discussed in Section III-D.

P_{lab}=2.912 GeV/c	T_{lab}=2.776 GeV	E_{cm}=2.524 GeV	
Cos θ_{cm}	-t	$P(\theta)$	$\Delta P(\theta)$
.909	.214	-.22	.10
.869	.306	-.11	.07
.834	.390	-.06	.08
.795	.481	.05	.08
.722	.651	.28	.15
.679	.752	-.27	.15
.619	.894	-.27	.17
.551	1.054	-.74	.15
.469	1.245	-.69	.14
.385	1.442	-.78	.14
.302	1.638	-.75	.21
.219	1.831	-.89	.23
.139	2.019	-.39	.42

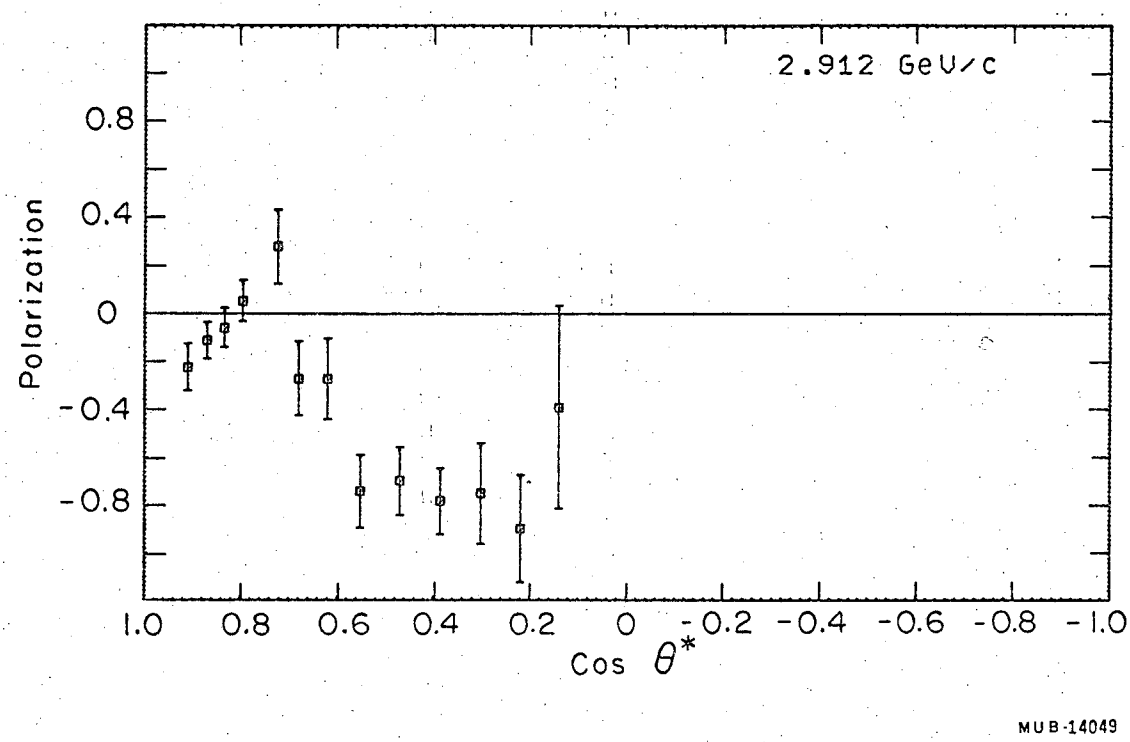

Fig. 15. Polarization in $\pi^- p$ scattering for an incident-pion momentum of 2.912 GeV/c. The errors shown are statistical only and do not include the systematic error discussed in Section III-D. The systematic error corresponds to an uncertainty of 8 percent in the target polarization. It results in an 8 percent uncertainty in the scale against which the polarization is measured.

Table XII. Polarization parameter $P(\theta)$ in $\pi^- p$ scattering. The error $\Delta P(\theta)$ is statistical only and does not include the systematic error discussed in Section III-D.

P_{lab} = 3.260 GeV/c	T_{lab} = 3.123 GeV		E_{cm} = 2.650 GeV
Cos θ_{cm}	-t	$P(\theta)$	$\Delta P(\theta)$
.914	.230	-.17	.10
.873	.337	-.04	.08
.827	.462	-.04	.07
.785	.572	.03	.13
.705	.785	.14	.15
.644	.949	.17	.17
.578	1.125	-.62	.17
.498	1.338	-.70	.15
.411	1.569	-.77	.17
.324	1.802	-.82	.27
.238	2.031	-.32	.44

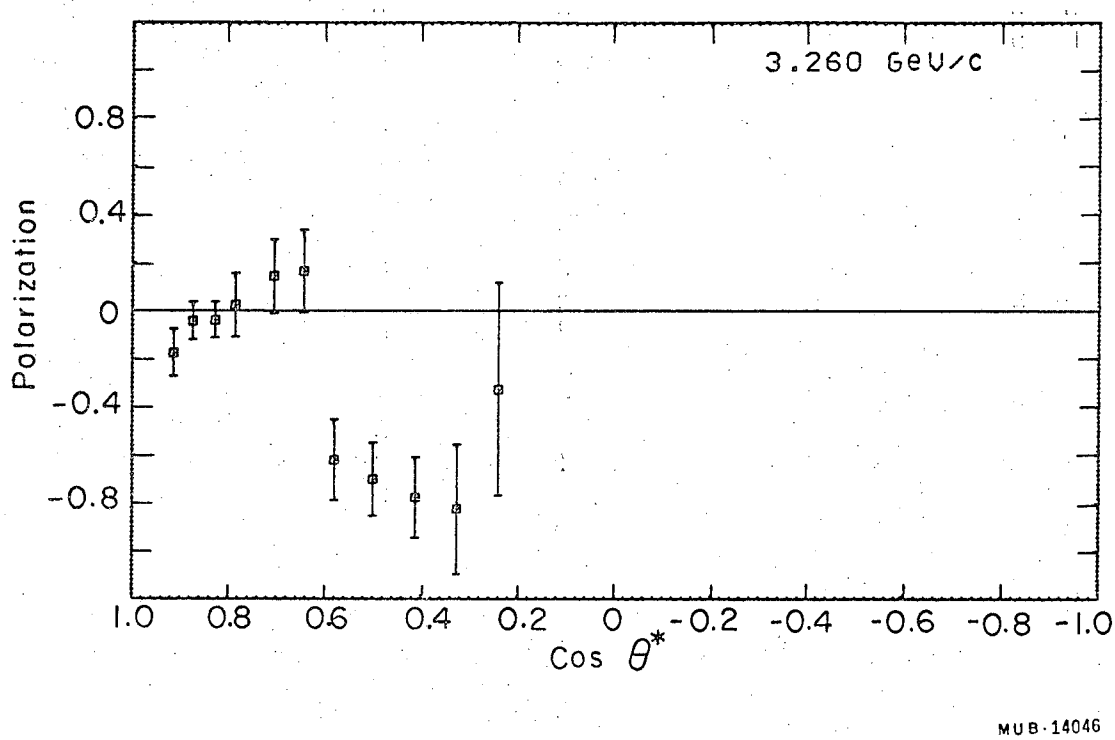

Fig. 16. Polarization in $\pi^- p$ scattering for an incident-pion momentum of 3.260 GeV/c. The errors shown are statistical only and do not include the systematic error discussed in Section III-D. The systematic error corresponds to an uncertainty of 8 percent in the target polarization. It results in an 8 percent uncertainty in the scale against which the polarization is measured.

V. DISCUSSION OF THE RESULTS

With the help of the polarization results presented in the previous section and the other available data on the πN system referred to in the Introduction, we have conducted a fairly extensive phase-shift analysis at several energies ranging from 490 to 1050 MeV. However, the preliminary state of this analysis does not allow us to draw very definite conclusions from the results obtained so far, so that only the general features and difficulties encountered will be discussed here. Before doing this, we will summarize the basic equations used in the phenomenological analysis of the pion-nucleon scattering.

A. Formalism

The scattering of a spinless particle (pion) by a spin-1/2 particle (nucleon) is conveniently described by a scattering matrix $M(\theta^*,k)$, which can be expressed in the form[32]

$$M(\theta^*,k) = f(\theta^*,k) + g(\theta^*,k)\vec{\sigma}\cdot\hat{n} \qquad \text{(V-1)}$$

where θ^* and k are the center-of-mass scattering angle and momentum, respectively, $\hat{n}$ is the normal to the scattering plane as defined in Section II-A, $\vec{\sigma}(\sigma_x,\sigma_y,\sigma_z)$ are the Pauli spin matrices operating on the spinors of the nucleons, and $f(\theta^*,k)$ and $g(\theta^*,k)$ are the non-spin-flip amplitude and the spin-flip amplitude, respectively. Each of the three elastic processes

$$\pi^+ + p \rightarrow \pi^+ + p$$

$$\pi^- + p \rightarrow \pi^- + p$$

$$\pi^- + p \rightarrow \pi^0 + n ,$$

is described by the three scattering matrices M_+ , M_- and M_o respectively. The charge-independence property of strong interactions relates the amplitudes for these reactions, so that all experimental observables can be expressed in terms of two amplitudes $M^T(\theta^*,k)$ for each value of the total isotopic spin: $T=1/2$ and $T=3/2$. Each matrix $M^T(\theta^*,k)$ is expressible in terms of amplitudes $f^T(\theta^*,k)$ and $g^T(\theta^*,k)$ as in Eq. V-1. Therefore, four independent amplitudes are required to describe the elastic πN scattering. A summary of the results is given in Table XIII.

Table XIII. Scattering amplitudes for pion-nucleon scattering

Process	Amplitude
$\pi^+ + p \to \pi^+ + p$	$M_+ = f_+ + g_+ \vec{\sigma}\cdot\hat{n} = M^{3/2}$
	$f_+ = f^{3/2}$; $g_+ = g^{3/2}$
$\pi^- + p \to \pi^- + p$	$M_- = f_- + g_- \vec{\sigma}\cdot\hat{n} = \frac{1}{3} M^{3/2} + \frac{2}{3} M^{1/2}$
	$f_- = \frac{1}{3} f^{3/2} + \frac{2}{3} f^{1/2}$
	$g_- = \frac{1}{3} g^{3/2} + \frac{2}{3} g^{1/2}$
$\pi^- + p \to \pi^o + n$	$M_o = f_o + g_o \vec{\sigma}\cdot\hat{n} = \frac{\sqrt{2}}{3} (M^{3/2} - M^{1/2})$
	$f_o = \frac{\sqrt{2}}{3} (f^{3/2} - f^{1/2})$
	$g_o = \frac{\sqrt{2}}{3} (g^{3/2} - g^{1/2})$

The experimentally measured quantities are:

Differential cross section: $I_o = |f|^2 + |g|^2$ (V-2)

Polarization parameter: $\vec{P} = P\hat{n} = \frac{2\,\mathrm{Re}(f^* g)}{|f|^2 + |g|^2}\,\hat{n}$ (V-3)

where the appropriate subscripts $(+,-,o)$ have been omitted. The two additional parameters, R and A, are linear combinations of the expressions $(|f|^2-|g|^2)$ and $\mathrm{Im}(f^* g)$. In order to measure these parameters, it is necessary to make a double scattering experiment with the first target polarized in the plane of the first scattering. No such target has been developed until now, so that, at the present time, the available experimental information comes from total cross-sections, differential cross-sections and polarization measurements.

The amplitudes f^T and g^T of Table XIII can further be expressed in terms of partial-wave amplitudes in the following way:

$$f^T(\theta^*,k) = \frac{1}{k}\sum_{\ell}\left[(\ell+1)f^T_{\ell+} + \ell\, f^T_{\ell-}\right]P_\ell(\cos\theta^*) \qquad \text{(V-4)}$$

$$g^T(\theta^*,k) = \frac{i\,\sin\theta^*}{k}\sum_{\ell}\left(f^T_{\ell+} - f^T_{\ell-}\right)\frac{d\,P_\ell(\cos\theta^*)}{d\,\cos\theta^*} \qquad \text{(V-5)}$$

where the P_ℓ's are Legendre polynomials and $f^T_{\ell\pm}$ are the partial-wave amplitudes for orbital angular momentum ℓ, total angular momentum $j = \ell \pm \frac{1}{2}$ and total isotopic spin T. The partial-wave amplitudes $f^T_{\ell\pm}$ are complex functions of energy (or momentum) and are conveniently parametrized in terms of phase-shifts $\delta^T_{\ell\pm}$ and absorption parameters $\eta^T_{\ell\pm}$ as

$$f^T_{\ell\pm} = \frac{\eta^T_{\ell\pm}\, e^{2\,i\,\delta^T_{\ell\pm}} - 1}{2\,i} \qquad \text{(V-6)}$$

In the following, we shall use the usual notation L_{2T2j} for the partial-wave amplitudes, where L is the spectroscopic symbol for orbital angular momentum; for example, S_{31} is the amplitude with $\ell = 0$, $T = \frac{3}{2}$, and $j = \frac{1}{2}$. Using Eqs. V-2 through V-6, the various observables can be expressed in terms of phase-shifts and absorption parameters, which are a convenient set of parameters for analyzing the experimental data.

B. Phase-Shift Analyses

The phase-shift analysis of the pion-nucleon system has been extended to 1 GeV by Bareyre et al.[20] and to 1.3 GeV by Donnachie et al.[22] The analysis of Bareyre et al. proceeded by performing random searches at each energy, assuming no specific energy dependence for the various amplitudes. They included S , P , D , and F waves in their fits, except at 950 MeV and 990 MeV where G waves were added. By starting the analysis from the lower energy region where a unique solution exists and requiring a smooth behaviour with energy of the various waves as the analysis was extended to higher energy, they were able to find one continuous solution whose main characteristic was the appearance of a complex structure of resonances at energies in the vicinity of 600 MeV and 900 MeV where bumps have been observed in total cross-section measurements. Their resulting solution indicates that the waves S_{11} , P_{11}

and D_{13} have a resonant behaviour around $T_\pi = 600$ MeV and that four waves are resonating in the neighborhood of $T_\pi = 900$ MeV: S_{11}, D_{15}, F_{15}, and S_{31}. The phase-shift analysis of Donnachie et al. makes use of partial-wave dispersion relations constraints for the small amplitudes (large ℓ) while the large partial waves are fitted without restriction. In the energy range up to 600 MeV, there is good agreement between the phase-shift solutions obtained by these two groups, but, above 600 MeV, only the behaviour of the higher partial waves seems reasonably unique and no set of phase-shifts can be considered firmly established, even though there is qualitative agreement between the various proposed solutions.

In an attempt to resolve these ambiguities and with the hope of establishing a unique solution in the energy region above 600 MeV, we made independent searches at 14 energies from $T_\pi = 490$ MeV to $T_\pi = 1050$ MeV, with intervals between successive energies of about 50 MeV. In addition to the differential cross-section and polarization data referred to in the Introduction, we have used in our searches the new polarization data presented here and in Reference 26. The real and imaginary parts of the forward amplitude, as calculated in Ref. 33, were also included as data points to be fitted. A normalization factor for each experiment was included as a parameter to be varied in the searches. For each energy, a starting set of phase-shifts was selected at random within a region in the parameter space extending on both sides of the solution given by Donnachie et al. For each wave, this starting region

spanned intervals from 60 to 100 degrees for the phases and from .2 to .8 for the absorption parameters, the largest freedom being given to the lower partial waves. We included S , P , D , F and G waves in all our searches. The random set of phase-shifts was then varied in order to minimize the total chisquare of the experimental data defined by

$$\chi^2 = \sum \left[\frac{Q^{calc} - Q^{exp}}{\Delta Q^{exp}} \right]^2$$

where Q^{exp} and Q^{calc} are the experimental and calculated values of the observable Q , respectively, and ΔQ^{exp} is the experimental uncertainty in the measured value of Q . The summation is over all experimental points. When a relative minimum of the χ^2 was reached, the corresponding new set of phase-shifts was then used as a starting point for a new search with a more stringent convergence criterion for the χ^2 . This procedure was repeated many times, in general about 40 times per energy. In this way, we obtained at each energy several different sets of phase-shifts, all with values of the χ^2 very close to each other and giving a good fit of the experimental data. Many of these solutions could not be rejected, either by the requirement of reasonable continuity with energy or by the statistical criterion of their χ^2 values. The differences between the various acceptable solutions at each energy are mainly confined to the S and P waves, while the higher waves are reasonably well defined and agree with those of Bareyre et al. and Donnachie et al. In addition, we performed searches using Bareyre's solution as a starting point and obtained a resulting solution

which at some energies differed appreciably from the original set. This is not surprising since we included new polarization data and used G waves in our fits. Already at 650 MeV, the influence of the G waves is not negligible, as most of our possible solutions have the G-wave phase small, but non-zero. Undoubtedly, the presence of G-vaves is a major factor in increasing the number of possible solutions, which cannot be reduced to a unique set by continuity.

It is therefore unlikely that a unique solution can be found with the amount of data presently available, without making use of theoretical information such as partial-wave dispersion relations, but even in that case the work of Donnachie et al. indicates that the remaining ambiguities cannot be resolved, especially those in S_{11} and P_{11}. Many of the solutions that we have obtained have radically different predictions for the charge-exchange polarization parameter, for which there is no measurement at the present time. With the help of charge-exchange polarization data, when they become available, and more precise information on inelastic processes, it is likely that a unique solution will be established for pion-nucleon scattering.

ACKNOWLEDGMENTS

I wish to express my deepest gratitude to Professor Owen Chamberlain, not only for his detailed supervision of this work, but also for his constant interest and advice throughout my graduate studies.

I owe much appreciation to Professor Herbert Steiner, whose dynamism and enthusiasm contributed much to the success of this experiment.

My thanks go to Dr. Leland Holloway for his constant efforts during the preparation and performance of this experiment. I am very grateful to Dr. Paul Grannis and Dr. Luc Valentin, particularly for their contributions to the data analysis.

Very special thanks go to my co-worker, Claiborne Johnson, for his close collaboration throughout this work. His aid in the data reduction and phase-shift analysis has been indispensable.

I wish to express my gratitude to Dr. John Arens, Dr. J. Brolley, Dr. Byron Dieterle, Dr. David Weldon, Raymond Fuzesy, William Gorn, Charles Morehouse, Michael Paciotti, Peter Robrish, and Stephen Rock for their contributions throughout the course of this experiment.

The constant assistance of the Bevatron operating crew and of the staff of the computer center of the Lawrence Radiation Laboratory is gratefully acknowledged.

I am indebted to the Belgian American Educational Foundation for havinggiven me a C.R.B. Fellowship for the first two years of my graduate studies.

Finally, I am very grateful to my wife, Marie-France, for her constant help and encouragement in these sometimes difficult years of graduate work.

APPENDIX

In section III-C, we obtained the least squares fit conditions:

$$\frac{\partial J}{\partial I_o} = \frac{\partial J}{\partial I_1} = 0 \tag{A-1}$$

where

$$J = \sum_i M_i \left[H_i - (I_o + I_1 p_i)\right]^2$$

and

$$H_i = \frac{N_i - B_i}{M_i} \tag{A-2}$$

$$I_1 = I_o P$$

$$B_i = bM_i .$$

From (A-1), one gets

$$\sum_i (N_i - B_i)p_i - I_o \sum_i M_i p_i - I_o P \sum_i M_i p_i^2 = 0$$

and

$$\sum_i (N_i - B_i) - I_o \sum_i M_i - I_o P \sum_i M_i p_i = 0$$

Solving for P, this yields

$$P = \frac{\sum_i (N_i - B_i)p_i - \langle p \rangle \sum_i (N_i - B_i)}{\langle p^2 \rangle \sum_i M_i H_i - \langle p \rangle \sum_i H_i M_i p_i} \tag{A-3}$$

where

$$\langle p \rangle = \frac{\sum_i M_i p_i}{\sum_i M_i} \tag{A-4}$$

and

$$< p^2 > = \frac{\sum_i M_i p_i^2}{\sum_i M_i} \tag{A-5}$$

Defining a new variable, q_i, by

$$q_i = p_i - < p >$$

(A-3) becomes

$$P = \frac{\sum_i (N_i - B_i)\, q_i}{< q^2 > \sum_i (N_i - B_i) - < p > \sum_i (N_i - B_i)\, q_i}$$

which can be written

$$P = \frac{\epsilon}{1 - \epsilon < p >} \tag{A-6}$$

where

$$\epsilon = \frac{\sum_i (N_i - B_i)\, q_i}{< q^2 > \sum_i (N_i - B_i)}$$

$$= \frac{\sum_i N_i q_i}{< q^2 > \left[\sum_i N_i - R \sum_j D_j \right]} \tag{A-7}$$

R is the ratio of coplanar to background counts in the off-elastic peak regions, as defined in section III-C, and D_j is the number of background counts in the elastic peak during the $j^{\underline{th}}$ run.

The statistical error in P is expressed by

$$[\Delta P]^2 = \left[\frac{\partial P}{\partial \epsilon}\Delta\epsilon\right]^2 + \left[\frac{\partial P}{\partial < p >}\Delta < p >\right]^2$$

The second term of this expression is very small, as can be easily verified, and its contribution can be neglected in the calculation of ΔP. Then

$$\Delta P = \frac{1}{[1 - < p > \epsilon]^2}\Delta\epsilon$$

with

$$\Delta\epsilon = \left\{ \sum_i \left(\frac{\partial\epsilon}{\partial N_i}\Delta N_i\right)^2 + \left(\frac{\partial\epsilon}{\partial R}\Delta R\right)^2 + \right.$$

$$+ \left(\frac{\partial\epsilon}{\partial(\sum_j D_j)}\Delta(\sum_j D_j)\right)^2 + \sum_i \left(\frac{\partial\epsilon}{\partial M_i}\Delta M_i\right)^2 +$$

$$\left. + \sum_i \left(\frac{\partial\epsilon}{\partial p_i}\Delta p_i\right)^2 \right\}^{\frac{1}{2}}$$

1) ΔN_i is the statistical uncertainty of the coplanar counts in the elastic peak: $\Delta N_i = \sqrt{N_i}$.

2) ΔR is the error in R due to the statistical uncertainty in the number of events in the off-elastic peak regions, used in the normalization of the background counts:

$$\Delta R = \left\{ \frac{\sum_i \sum_{NE} N_i}{\sum_j \sum_{NE} D_j} \right\} \left\{ \frac{1}{\sum_i \sum_{NE} N_i} + \frac{1}{\sum_j \sum_{NE} D_j} \right\}^{\frac{1}{2}}$$

3) $\Delta(\sum_j D_j)$ is the statistical error due to the background counts, D_j, in the elastic peak:

$$\Delta(\sum_j D_j) = \sqrt{\Sigma_j D_j} \ .$$

4) ΔM_i is the error in the number of monitor counts:

$$\Delta M_i = \sqrt{M_i} \ .$$

5) Δp_i is the error in the target polarization for the $i^{\underline{th}}$ run. This error is due to random fluctuations of the target polarization caused by changes in the polarization detection system or fluctuations of the magnetic field and microwave power sent to the crystals. This error was estimated to be small and was included in the systematic error.

REFERENCES

1. Young S. Kim, Phys. Rev. 129, 862 (1963).

2. P. Bareyre, C. Bricman, M. J. Longo, G. Valladas, G. Villet, G. Bizard, J. Duchon, J. M. Fontaine, J. P. Patry, J. Seguinot, and J. Yonnet, Phys. Rev. Letters 14, 878 (1965).

3. T. J. Devlin, J. Solomon, and G. Bertsch, Phys. Rev. Letters 14, 1031 (1965).

4. J. C. Brisson, J. F. Detoeuf, P. Falk-Vairant, L. van Rossum, and G. Valladas, Nuovo Cimento 19, 210 (1961).

5. T. J. Devlin, B. J. Moyer, and V. Perez-Mendez, Phys. Rev. 125, 690 (1962).

6. A. N. Diddens, E. W. Jenkins, T. F. Kycia, and K. F. Riley, Phys. Rev. Letters 10, 262 (1963).

7. A. Stirling, Thesis, Saclay report No. CEA-R2838 (1966).

8. N. P. Klepikov, V. A. Mescheryakov, and S. N. Sokolov, Analysis of Experimental Data on the Total Cross Sections for Pion-Proton Interaction, (Joint Inst. for Nuclear Research, Dubna, USSR, 1960). A compilation of total cross-section data; the references are cited in the article.

9. P. Bareyre, C. Bricman, G. Valladas, G. Villet, G. Bizard, and J. Seguinot, Phys. Letters 8, 137 (1964).

10. A. Citron, W. Galbraith, T. F. Kycia, B. A. Leontic, R. H. Phillips, and A. Rousset, Phys. Rev. Letters 13, 205 (1964).

11. A. Donnachie and J. Hamilton, Phys. Rev. 133, B1053 (1964) and references cited therein.

12. J. A. Helland, T. J. Devlin, D. E. Hagge, M. J. Longo, B. J. Moyer, and C. D. Wood, Phys. Rev. 134, B1062 (1964).

J. A. Helland, C. D. Wood, T. J. Devlin, D. E. Hagge, M. J. Longo, B. J. Moyer, and V. Perez-Mendez, Phys. Rev. 134, B1079 (1964).

13. P. M. Ogden, D. E. Hagge, J. A. Helland, M. Banner, J-F Detoeuf, and J. Teiger, Phys. Rev. 137, B1115 (1965).

14. P. J. Duke, D. P. Jones, M. A. R. Kemp, P. G. Murphy, J. D. Prentice, and J. J. Thresher, Phys. Rev. 149, 1077 (1966).

15. F. Bulos, R. E. Lanou, A. E. Pifer, A. M. Shapiro, M. W. Idgoff, R. Pavini, A. E. Brenner, C. A. Bordner, M. E. Law, E. E. Ronst, K. Strauch, J. Szymanski, P. Bastien, B. B. Brabson, Y. Eisenberg, B. T. Feld, V. K. Fischer, I. A. Pless, L. Rosenson, R. K. Yamamoto, G. Calvelli, L. Guerriero, G. A. Saladin, A. Tomasin, L. Ventura, G. Voci, F. Waldner, Phys. Rev. Letters 13, 558 (1964);L. Guerriero, Proc. Roy. Soc. (London) A289, 471 (1966).

16. Charles Chiu, Pion-Proton Charge Exchange Scattering 500-1300 MeV (Ph.D. thesis), UCRL-16209, (1965) (to be published).

17. H. H. Atkinson, C. R. Cox, P. J. Duke, K. S. Heard, D. P. Jones, M. A. R. Kemp, P. G. Murphy, J. D. Prentice, and J. J. Thresher, Proc. Roy. Soc. (London) A289, 449 (1966) and Phys. Rev. Letters 15, 468 (1965).

18. R. D. Eandi, T. J. Devlin, R. W. Kenney, P. G. McManigal, and B. J. Moyer, Phys. Rev. 136, B536 (1964) and Phys. Rev. 136, B1187 (1964).

19. P. Bareyre, C. Bricman, M. J. Longo, G. Valladas, G. Villet, G. Bizard, J. Duchon, J. M. Fontaine, J. P. Patry, J. Seguinot, and J. Yonnet, Phys. Rev. Letters 14, 198 (1965) and Phys. Rev. Letters 14, 878 (1965).

20. P. Bareyre, C. Bricman, A. V. Stirling, and G. Villet, Phys. Letters 18, 342 (1965).

21. R. J. Cence, Phys. Letters 20, 306 (1966).

22. P. Auvil, A. Donnachie, A. T. Lea, and C. Lovelace, Phys. Letters 12, 76 (1964); 19, 148 (1965).

A. Donnachie, R. G. Kirsopp, A. T. Lea, and C. Lovelace, "Pion-nucleon phase shifts up to 1311 MeV", presented at the International Conference on High Energy Physics, Berkeley (1966).

23. L. D. Roper, Phys. Rev. Letters 12, 340 (1964); L. D. Roper, R. M. Wright, and B. T. Feld, Phys. Rev. 138, B190 (1965).

L. D. Roper and R. M. Wright, Phys. Rev. 138, B921 (1965).

24. M. H. Hull and F. C. Lin, Phys. Rev. 139, B630 (1965).

25. B. H. Bransden, P. J. O'Donnell and R. G. Moorhouse, Phys. Letters 11, 339 (1964); Phys. Rev. 139, B1566 (1965); Proc. Roy. Soc. (London) A289, 538 (1966); Phys. Letters 19, 420 (1965).

26. Owen Chamberlain, Michel J. Hansroul, Claiborne H. Johnson, Jr.,

Paul D. Grannis, Leland E. Holloway, Luc Valentin, Peter R. Robrish, and Herbert M. Steiner, Phys. Rev. Letters 17, 975 (1966).

27. G. Shapiro, Progr. in Nucl. Techn. and Instrumentation, North-Holland, January 1964.

28. F. Betz, J. Arens, O. Chamberlain, H. Dost, P. Grannis, M. Hansroul, L. Holloway, C. Schultz, and G. Shapiro, Phys. Rev. 148, 1289 (1966).

29. David Cheng, Nucleon-Nucleon Polarization at 700, 600, 500 and 400 MeV (Ph. D. thesis) UCRL-11962 (July 1965) (to be published).

30. Homer A. Neal, Jr., Technical Report No. 23, University of Michigan, Ann Arbor (unpublished).

31. S. Suwa, A. Yokosawa, N. Booth, R. Esterling, and R. Hill, Phys. Rev. Letters 15, 560 (1965).

32. J. Ashkin, Nuovo Cimento Suppl. 14, 221 (1959).

33. J. Baacke, private communication.

G. Höhler, G. Ebel, and J. Giesecke, Zeitschrift für Physik 180, 430 (1964).

This report was prepared as an account of Government sponsored work. Neither the United States, nor the Commission, nor any person acting on behalf of the Commission:

A. Makes any warranty or representation, expressed or implied, with respect to the accuracy, completeness, or usefulness of the information contained in this report, or that the use of any information, apparatus, method, or process disclosed in this report may not infringe privately owned rights; or

B. Assumes any liabilities with respect to the use of, or for damages resulting from the use of any information, apparatus, method, or process disclosed in this report.

As used in the above, "person acting on behalf of the Commission" includes any employee or contractor of the Commission, or employee of such contractor, to the extent that such employee or contractor of the Commission, or employee of such contractor prepares, disseminates, or provides access to, any information pursuant to his employment or contract with the Commission, or his employment with such contractor.